is much larger than the value reported previously of $k = 4.5 \times 10^{-10}$.

$$CCCN^+ + C_2N_2 \longrightarrow C_4N_2^+ + CN \quad (0.20) \quad (20a)$$
$$\longrightarrow C_3N^+ \cdot C_2N_2 \quad (0.80) \quad (20b)$$

Conclusion

Electron impact of HC_3N generates two isomers of C_3N^+. The more abundant form is $CCCN^+$, and it is considered that the less abundant isomer is more likely to be c-C_3N^+ than $CCNC^+$. A notable finding of this work was that the lower energy isomer, $CCCN^+$, was found to be more reactive than the higher energy isomer designated c-C_3N^+.

The different reactivities of the two isomers can be rationalized in terms of the structures proposed for each isomer. $CCCN^+$, because of its carbene character, might be anticipated to be reactive. Carbene attack on the neutral reagent, followed by some rearrangement, can explain the formation of many products. c-C_3N^+, on the other hand, exhibits activation barriers in most of its reactions which are probably linked with ring opening requirements. The much lower reactivity of the cyclic isomer is also consistent with the lower reactivity observed for the cyclic isomers of the hydrocarbon ions such as $C_3H_2^+$ and $C_3H_3^+$.

Acknowledgment. We thank Dr. Alan Happer for helpful discussions, Mr. Barry Wells for the preparation of CH_3C_3N, and Mr. Paul Wilson for assistance with some of the measurements reported here. We also thank one of the referees for their comments leading to the inclusion of Tables III and IV.

The S_N2 Identity Exchange Reaction $ClCH_2CN + Cl^- \rightarrow Cl^- + ClCH_2CN$: Experiment and Theory

Brian D. Wladkowski, Kieran F. Lim,[†,1] Wesley D. Allen,* and John I. Brauman*

Contribution from the Department of Chemistry, Stanford University, Stanford, California 94305-5080, and Department of Chemistry, University of New England, Armidale NSW 2351, Australia. *Received January 22, 1992. Revised Manuscript Received April 29, 1992*

Abstract: The rate of substitution for the title reaction has been measured in the gas phase using Fourier transform ion cyclotron resonance (FT-ICR) spectrometry. The value of the observed rate coefficient is found to be $3.3 \pm 1.0 \times 10^{-10}$ cm^3 s^{-1} at 350 K, a reaction rate approximately one-tenth of the electrostatic ion–molecule collision rate. The experimental complexation energy for the formation of the intermediate ion–molecule complex, $[ClCH_2CN \cdot Cl]^-$, has also been measured using FT-ICR spectrometry by bracketing the associated equilibrium constant relative to values for compounds with known chloride affinities. Hence, $\Delta H^\circ_{350} = -19.4$ kcal mol^{-1} is obtained for the enthalpy of complexation at 350 K. By applying RRKM theory with the microcanonical variational transition state (μVTS) criterion to model the reaction, it is deduced that the observed experimental efficiency corresponds to an S_N2 transition state 5.9 kcal mol^{-1} *below* the separated reactants, or 13.5 kcal mol^{-1} above the intermediate ion–molecule complex. To further elucidate the potential surface for the title reaction and to provide data for the RRKM analysis, high-level ab initio quantum chemical results have been determined. In particular, the geometric structures, relative energies, and vibrational frequencies of four salient stationary points on the potential surface (separated reactants, two ion–dipole complex structures, and the S_N2 transition state) have been investigated at various levels of theory ranging from 3-21G RHF to 6-31+G(d,p) MP4 to TZ3P+(2f,d)+diffuse MP2. The ab initio results predict the ion–dipole complex and the S_N2 transition state to lie 18.4 and 6.9 kcal mol^{-1}, respectively, below the separated reactants, in excellent agreement with experiment. For comparison, improved theoretical predictions are obtained for the CH_3Cl/Cl^- system, viz. a complexation energy of 10.6 kcal mol^{-1} and an S_N2 barrier 1.8 kcal mol^{-1} *above* the separated reactants. Qualitative bonding models describing the effect of α substitution on the stability of S_N2 transition states are subsequently analyzed using the ab initio results for the CH_3Cl/Cl^- and $ClCH_2CN/Cl^-$ systems. The α effect in these systems appears not to arise from "resonance" effects in the transition state.

I. Introduction

Detailed experimental studies in the early 1950s established the fundamental mechanism for bimolecular nucleophilic substitution (S_N2) reactions in solution and laid the groundwork for much of what is known today about this pervasive chemical process.[2,3] Since the early 1970s, much work has focused on the characteristics of these reactions in the gas phase in order to more clearly understand both "intrinsic" and solvent effects.[4-14] In the study of intrinsic features of S_N2 processes, identity exchange reactions, in which the entering and leaving groups are the same, are especially useful. However, S_N2 identity exchange in the gas phase is often too slow to be measured because of large activation barriers. Nevertheless, gas-phase investigations of such processes have recently become experimentally realizable through the discovery of sufficiently fast reactions, and a few examples of chloride- and bromide-ion exchange have been documented.[15-17]

The α-substitution effect and the applicability of Marcus theory[18] to S_N2 systems are two issues for which a more complete

[†] Department of Chemistry, University of New England.

(1) Archbishop Mannix Traveling Scholar, 1988–1990.
(2) Streitwieser, A. *Solvolytic Displacement Reactions*; McGraw-Hill: New York, 1962.
(3) Lowry, T. H.; Richardson, K. S. *Mechanism and Theory in Organic Chemistry*, 3rd ed.; Harper and Row: New York, 1987.
(4) Brauman, J. I.; Olmstead, W. N.; Lieder, C. A. *J. Am. Chem. Soc.* **1974**, *96*, 4030.
(5) Olmstead, W. N.; Brauman, J. I. *J. Am. Chem. Soc.* **1977**, *99*, 4219.
(6) Pellerite, M. J.; Brauman, J. I. *J. Am. Chem. Soc.* **1980**, *102*, 5993.
(7) Pellerite, M. J.; Brauman, J. I. *J. Am. Chem. Soc.* **1983**, *105*, 2672.
(8) Dodd, J. A.; Brauman, J. I. *J. Am. Chem. Soc.* **1984**, *106*, 5356.
(9) Dodd, J. A.; Brauman, J. I. *J. Phys. Chem.* **1986**, *90*, 3559.
(10) Han, C.-C.; Dodd, J. A.; Brauman, J. I. *J. Phys. Chem.* **1986**, *90*, 471.
(11) Brauman, J. I.; Dodd, J. A.; Han, C.-C. *Adv. Chem. Ser.* **1987**, *No. 215*, Chapter 2.
(12) Caldwell, G.; Magnera, T. F.; Kebarle, P. *J. Am. Chem. Soc.* **1984**, *106*, 959.
(13) Tanaka, K.; Mackay, G. I.; Payzant, J. D.; Bohme, D. K. *Can. J. Chem.* **1976**, *54*, 1643.

0002-7863/92/1514-9136$03.00/0

understanding of intrinsic structure–reactivity relationships is sought through the measurement and quantitative modeling of identity exchange reactions. In solution, a π system in the α position relative to the S_N2 reaction center can increase the reaction rate by orders of magnitude relative to the unsubstituted species. By using gas-phase thermoneutral reactions to probe this α effect, complications arising from the solvent and the reaction thermodynamics are eliminated, and the relationship between chemical structure and activation energy is more clearly exposed. Moreover, because the potential surfaces for identity exchange reactions are symmetric, theoretical analyses are considerably simplified. Marcus theory has proved useful in the analysis of a variety of gas- and solution-phase processes, including S_N2 reactions. For a given substrate, the activation energies for S_N2 cross reactions within a group of nucleophiles can be predicted via Marcus theory provided the reaction exothermicities are known as well as the intrinsic activation energies for the component identity exchange reactions. The experimental verification of the internal consistency of the Marcus expression is an unrealized goal, although this issue has been addressed to some extent by ab initio quantum chemical methods.[19]

The resolution of intrinsic structure–reactivity relationships in S_N2 reactions requires *quantitative* energetic information about the potential energy surfaces of concern. An integral part of the experimental effort toward this goal is the application of statistical theories to interpret kinetic data. Rice–Ramsperger–Kassel–Marcus (RRKM) theory[20-28] has been used extensively to interpret the kinetic results of ion–molecule reactions, including S_N2 reactions.[5,7-9,11,12,26,29-35] Microcanonical variational transition-state (μVTST) RRKM theory[23,24,26,32,36-48] gives reasonable improvements over simple RRKM theory, especially for ion–molecule systems. The results obtained from μVTST theory are generally consistent with experimental observations, allowing the determination of the rates of many reactions a priori. There are, however, very few studies which justify in a rigorous way, the implementation of statistical theories to model gas-phase S_N2 reactions.[33,49]

Perhaps the simplest S_N2 identity exchange reaction is that of chloride ion with methyl chloride:

$$CH_3{}^{35}Cl + {}^{37}Cl^- \rightarrow {}^{35}Cl^- + CH_3{}^{37}Cl \qquad (1)$$

DePuy, Bierbaum, and co-workers[15,16] have obtained an accurate experimental value for the rate of this reaction using a flowing afterglow (FA) apparatus and found it to be exceedingly small. Because of its simplicity and also because it represents in some ways the prototypical S_N2 reaction, eq 1 has been the topic of numerous theoretical studies using ab initio quantum chemical techniques.[49-53] The theoretical investigations of eq 1 also include the use of both simple[50] and variational transition-state theory,[49] as well as classical trajectory calculations.[54-56] Although the application of statistical theories gives reasonable agreement with the experimental rate,[49,50] the trajectory calculations of Vande Linde and Hase show definite non-RRKM behavior in the reaction dynamics.[54-56] The reason for this behavior is not clear. It may be related to the small number of vibrational modes in the system or to the relatively high activation barrier that extends 1 to 5 kcal mol^{-1} above the energy of the separated reactants,[49-53] which ultimately leads to a low reaction efficiency. Neither of these features is typical of a large number of more reactive ion–molecule systems.

The purpose of this paper is to present both experimental and theoretical work on a model thermoneutral S_N2 system to gain further insight into the details of general S_N2 reactions. Arguably, the system represented in eq 1 is sufficient for this purpose. It is not clear, however, that this reaction is an optimal one for study, either experimentally or theoretically, for reasons mentioned above. Consequently, the identity S_N2 exchange reaction of chloride ion with chloroacetonitrile, eq 2, was chosen for investigation.

$$^{35}ClCH_2CN + {}^{37}Cl^- \rightarrow {}^{35}Cl^- + {}^{37}ClCH_2CN \qquad (2)$$

This reaction is ideal for study in that it is fast, has no side reactions, and has a rate which can be measured accurately, eliminating problems due to small amounts of impurities. Indeed, the rate of substitution for this reaction has been measured previously by Bierbaum, DePuy, and co-workers.[17] The system is still small enough, however, that high-quality ab initio studies can be performed to obtain quantitative results for the properties of stationary points along the reaction pathway. Moreover, because the reaction in eq 2 is fast and has a relatively small S_N2 activation barrier, it is probably more typical than eq 1 of a general class of somewhat slow, but still measurable, ion–molecule reactions.

To facilitate a clear presentation of the diverse issues addressed in this paper, the results are presented and discussed in three main

(14) Chandrasekhar, J.; Smith, S. F.; Jorgensen, W. L. *J. Am. Chem. Soc.* **1985**, *107*, 154.
(15) Barlow, S. E.; Van Doren, J. M.; Bierbaum, V. M. *J. Am. Chem. Soc.* **1988**, *110*, 7240.
(16) Van Doren, J. M.; DePuy, C. H.; Bierbaum, V. M. *J. Phys. Chem.* **1989**, *93*, 1130.
(17) DePuy, C. H.; Gronert, S.; Mullin, A.; Bierbaum, V. M. *J. Am. Chem. Soc.* **1990**, *112*, 8650.
(18) Marcus, R. A. *Annu. Rev. Phys. Chem.* **1964**, *15*, 155.
(19) Wolfe, S.; Mitchell, D. J.; Schlegel, H. B. *J. Am. Chem. Soc.* **1981**, *103*, 7694.
(20) Marcus, R. A. *J. Chem. Phys.* **1952**, *20*, 359.
(21) Marcus, R. A.; Hase, W. L.; Swamy, K. N. *J. Phys. Chem.* **1984**, *88*, 6717.
(22) Robinson, P. J.; Holbrook, K. A. *Unimolecular Reactions*; Wiley-Interscience: London, 1972.
(23) Forst, W. *Theory of Unimolecular Reactions*; Academic Press: New York, 1973.
(24) Gilbert, R. G.; Smith, S. C. *Theory of Unimolecular and Recombination Reactions*; Blackwells Scientific: Oxford, 1990.
(25) Forst, W. *J. Chim. Phys.* **1990**, *87*, 715.
(26) Smith, S. C.; McEwan, M. J.; Gilbert, R. G. *J. Chem. Phys.* **1989**, *90*, 1630.
(27) Zhu, L.; Hase, W. L. *Chem. Phys. Lett.* **1990**, *175*, 117.
(28) Steinfeld, J. I.; Francisco, J. S.; Hase, W. L. *Chemical Kinetics and Dynamics*; Prentice Hall: Englewood Cliffs, 1989.
(29) Farneth, W. E.; Brauman, J. I. *J. Am. Chem. Soc.* **1976**, *98*, 7891.
(30) Meyer, F. K.; Pellerite, M. J.; Brauman, J. I. *Helv. Chim. Acta* **1981**, *64*, 1058.
(31) Magnera, T. F.; Kebarle, P. In *Ionic Processes in the Gas Phase*; Almoster Ferreira, M. A., Ed.; D. Reidel: Dordrecht, 1984; p 135.
(32) Smith, S. C.; McEwan, M. J.; Gilbert, R. G. *J. Phys. Chem.* **1989**, *93*, 8142.
(33) Merkel, A.; Havlas, Z.; Zahradník, R. *J. Am. Chem. Soc.* **1988**, *110*, 8355.
(34) Verboom, G. M. L.; Meisels, G. G. *J. Chem. Phys.* **1978**, *68*, 2714.
(35) Meisels, G. G.; Verboom, G. M. L.; Weiss, M. J.; TaCheng, H. *J. Am. Chem. Soc.* **1979**, *101*, 7189.
(36) Chesnavich, W.; Bowers, M. T. In *Gas Phase Ion Chemistry*; Bowers, M. T., Ed.; Academic Press, New York, 1979; Vol. 1, p 119.
(37) Chesnavich, W. J.; Su, T.; Bowers, M. T. *J. Chem. Phys.* **1980**, *72*, 2641.
(38) Chesnavich, W. J.; Bass, L.; Su, T.; Bowers, M. T. *J. Chem. Phys.* **1981**, *74*, 2228.
(39) Bass, L.; Chesnavich, W. J.; Bowers, M. T. *J. Am. Chem. Soc.* **1979**, *101*, 5493.
(40) Garrett, B. C.; Truhlar, D. G. *J. Chem. Phys.* **1979**, *70*, 1593.
(41) Truhlar, D. G.; Garrett, B. C. *Acc. Chem. Res.* **1980**, *13*, 440.
(42) Klippenstein, S. J.; Marcus, R. A. *J. Phys. Chem.* **1988**, *92*, 3105.
(43) Miller, W. H. *J. Chem. Phys.* **1976**, *65*, 2216. For a more recent review see: Miller, W. H. *J. Phys. Chem.* **1983**, *87*, 3811.
(44) Quack, M.; Troe, J. *Ber. Bunsenges. Phys. Chem.* **1974**, *78*, 240.
(45) Quack, M.; Troe, J. *Int. Rev. Phys. Chem.* **1981**, *1*, 97.
(46) Greenhill, P. G.; Gilbert, R. G. *J. Phys. Chem.* **1986**, *90*, 3104.
(47) Smith, S. C.; Gilbert, R. G. *Int. J. Chem. Kinet.* **1988**, *20*, 307.
(48) Smith, S. C.; Gilbert, R. G. *Int. J. Chem. Kinet.* **1988**, *20*, 979.
(49) Vande Linde, S. R.; Hase, W. L. *J. Phys. Chem.* **1990**, *94*, 2778.
(50) Tucker, S. C.; Truhlar, G. G. *J. Phys. Chem.* **1989**, *93*, 8138.
(51) Vetter, R.; Zülicke, L. *J. Am. Chem. Soc.* **1990**, *112*, 5136.
(52) Shi, Z.; Boyd, R. *J. Am. Chem. Soc.* **1990**, *112*, 6789.
(53) Keil, F.; Ahlrichs, R. *J. Am. Chem. Soc.* **1976**, *98*, 4789.
(54) Hase, W. L. *J. Phys. Chem.* In press.
(55) Vande Linde, S. R.; Hase, W. L. *J. Am. Chem. Soc.* **1989**, *111*, 2349.
(56) Vande Linde, S. R.; Hase, W. L. *J. Phys. Chem.* **1990**, *94*, 6148.

sections (II–IV), which can in large part be read independently. In Section II, a experimental confirmation of the previous flowing afterglow measurement of the identity exchange rate for eq 2 is achieved using Fourier transform ion cyclotron resonance (FT-ICR) spectrometry. The chloride affinity corresponding to the intermediate ion–molecule complexation energy has also been measured for this reaction, and the result is discussed in terms of general principles of ion–molecule binding. In Section III, the reaction of eq 2 is modeled using microcanonical variational transition-state (μVTST) RRKM theory, and the observed rate is used in conjunction with the complexation energy to obtain an activation energy for substitution. In Section IV, extensive ab initio quantum chemical studies of highest quality are reported, in which the salient features of the surface are explored using several basis sets and the effects of electron correlation are considered in detail. Various qualitative bonding models for the intermediate ion–molecule complex and the S_N2 transition state are analyzed, with particular emphasis on α-substituent effects.

II. Experimental Investigation

A. Methods. (a) Materials. All chemicals were obtained from commercial sources (chloroacetonitrile, methanol, and methyl chloroformate from Aldrich; sulfur dioxide from Matheson). Most samples were used directly and without further purification. Fresh samples were introduced into the system each day to circumvent systematic problems due to impurities. All samples were subjected to multiple (at least three) freeze–pump–thaw cycles before being drawn into the high-vacuum apparatus.

(b) Instrumentation. All experiments were performed with a Fourier transform IonSpec FTMS-2000 ion cyclotron resonance (FT-ICR) spectrometer. Details of the experimental apparatus can be found elsewhere.[57,58] Briefly, experiments were performed in a rectangular cell (approximately 1 × 1 × 1.5 in.) in which the ions were trapped with magnetic fields in the range 0.8–1.2 T. Background pressures were in the range 0.8–2.0 × 10^{-8} Torr. Standard notched ejection techniques were used to remove unwanted ions from the detection region of the ICR cell and thereby isolate the ions of interest, which were subsequently detected via impulse excitation techniques.

During the experiments, pressures of neutral species within the ICR cell were monitored with an ion gauge (Varian 844), which was calibrated daily against a capacitance manometer (MKS 170 Baratron with a 315BH-1 head). The reaction of methane radical cation with methane ($CH_4^+ + CH_4 \rightarrow CH_5^+ + CH_3$), which has a rate coefficient that is well known, was used to verify that the absolute pressure readings were sufficiently accurate. All experiments were carried out at a temperature estimated to be 350 K.[57]

(c) Kinetic Data Collection. The primary ion, Cl^-, was produced in the ICR cell directly from chloroacetonitrile by dissociative electron attachment using thermally generated electrons. Generation of the proper isotopic ratio ($^{35}Cl/^{37}Cl \approx 3$) was confirmed before each kinetic run. The data collection was initiated with primary ion formation for 5–10 ms followed by ejection of free electrons for 10–30 ms. After a short time delay (ca. 30–50 ms) to aid in ion thermalization, one of the chloride-ion isotopes[59] was ejected from the detection region. The ion signals of both isotopes were then measured using signal averaging (20–50 times) at 7–15 different increments of time as the equilibrium chloride–ion isotopic ratio was re-established over a period of ca. 800–2000 ms, depending on the pressure of $ClCH_2CN$ in the cell. Kinetic runs were repeated on different days and at a variety of pressures of $ClCH_2CN$ (2 × 10^{-7}–2 × 10^{-6} Torr); the results presented here comprise an average of all runs. In Figure 1, data for a typical kinetic run are plotted. The error in the kinetic measurements is believed to be determined by the error in the pressure measurements, which are reproducible within 20–30%. Impurities within samples or those generated within vacuum systems often introduce errors in ICR kinetic measurements. Here the problem is ameliorated because the identity substitution of Cl^- with $ClCH_2CN$ is quite rapid and hence less sensitive to the presence of reactive impurities.

(d) Thermodynamic Data Collection. At the pressures within the ICR spectrometer, ion–molecule complex formation is difficult or impossible from direct association via three-body stabilization. Thus, the method

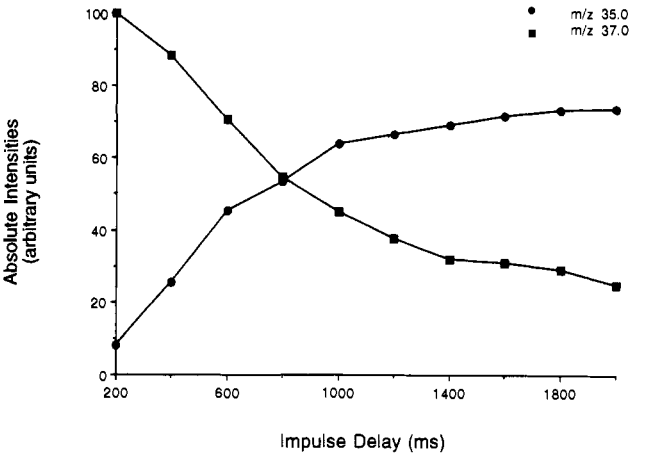

Figure 1. Representative data of the absolute ion intensities as a function of time for the S_N2 reaction $^{35}ClCH_2CN + {}^{37}Cl^- \rightarrow {}^{35}Cl^- + {}^{37}ClCH_2CN$.

Scheme I

$$CH_3OCOCl + e^- \rightarrow Cl^- + CH_3OCO^\cdot \quad (3)$$

$$CH_3OCOCl + Cl^- \rightarrow CH_3Cl + ClCO_2^- \quad (4)$$

$$M + ClCO_2^- \rightarrow [M\cdot Cl]^- + CO_2 \quad (5)$$

$$M = (CH_3OCOCl,\ SO_2,\ CH_3OH,\ \text{or}\ ClCH_2CN)$$

of Larson and McMahon[60] was used here for the generation of chloride–ion/neutral complexes (as shown in Scheme I). Once conditions to produce sufficient amounts of $ClCO_2^-$ were established, chloroacetonitrile was introduced into the ICR cell followed by either SO_2 or CH_3OH, bracketing compounds with known chloride affinities somewhat higher and lower, respectively, than that of $ClCH_2CN$. Ion signals over the appropriate mass range were measured and averaged (20–50 times) at selected time increments until equilibrium was reached (after ca. 500–3000 ms) between the chloride-ion complexes of $ClCH_2CN$ and the bracketing species. Sums of final ion intensities of all chlorine isotopomers of the ion–molecule complexes were used to determine equilibrium constants for chloride-ion exchange. Pressure measurements to determine the individual concentrations of neutral species were performed as described above; total pressures in these experiments ranged from 2 × 10^{-7} to 2 × 10^{-6} Torr. Equilibrium measurements were made at a variety of pressures and on different days.

B. Experimental Results. (a) Kinetics. The observed rate constant for eq 2 was obtained by the method of Eyler and Richardson,[61] in which *ratios* of ion intensities are analyzed as a function of time rather than absolute ion signals. As long as the relative rates of reactant and product ion loss are nearly equivalent, which is an excellent approximation for identity exchange reactions, ion-loss errors are eliminated with this technique, thus making it preferred for systems with a very slow rate of exchange. The detection limit for chloride identity exchange reactions has been lowered substantially by this technique and is now in the range of 2 × 10^{-13} cm^3 s^{-1} for our ICR instrument. Thus, a wide variety of identity substitution reactions can now be investigated which were inaccessible in the past. The rate expression for the analysis as applied to the system of interest here is given by:[61]

$$\ln\left[\frac{R_t - R_\infty}{R_t + 1}\right] = -k_{obs}Pt \quad (6)$$

where P is the total pressure, R_t is the ratio of ion intensities ($[^{35}Cl^-]/[^{37}Cl^-]$) at some time t, R_∞ is the ratio of ion intensities at infinite time (i.e., the natural abundance ratio), and k_{obs} represents the observed rate coefficient of eq 2. In Figure 2 the application of eq 6 to the set of experimental data given in Figure 1 is shown.

The observed rate coefficient for eq 2 at 350 K is given in Table I along with the previous results of DePuy, Bierbaum, and co-workers[17] at 300 K. The uncertainty represents one standard deviation. Also given in Table I are the calculated capture rates, k_{cap}, obtained from various theories, and the corresponding efficiency ($\Phi = k_{obs}/k_{cap}$) for the reaction (see Section III).

(b) Thermodynamics. The complexation energy for $[ClCH_2CN\cdot Cl]^-$, which corresponds to the chloride affinity (CA) shown in eq 7, was

(57) Han, C.-C.; Brauman, J. I. *J. Am. Chem. Soc.* **1989**, *111*, 6491.
(58) Riveros, J. M.; Jose, S. M.; Takashima, K. *Adv. Phys. Org. Chem.* **1985**, *21*, 197.
(59) In this particular case, $^{35}Cl^-$ was ejected. The rate was identical within experimental uncertainty no matter which isotope was ejected. Ejecting $^{35}Cl^-$ is preferred since initially the system is farther away from equilibrium. This is useful when measuring very slow identity exchange reactions.
(60) Larson, J. W.; McMahon, T. B. *Can. J. Chem.* **1984**, *62*, 675.
(61) Eyler, J. R.; Richardson, D. E. *J. Am. Chem. Soc.* **1985**, *107*, 6130.

Table I. Kinetic Data for $^{35}ClCH_2CN + {}^{37}Cl^- \rightarrow {}^{35}Cl^- + {}^{37}ClCH_2CN$

method	$k_{obs}(exp)^a$	$k_{cap}(ADO)^{a,b}$	$k_{cap}(SC)^{a,b}$	$k_{cap}(\mu VTST)^a$	$\Phi_{exp}(\%)^c$	ΔE_{diff}^d
FT-ICR (350 K)[e]	3.3 ± 1.0	23.2	29.4	43.5	7.6 – 14.2	−5.9 ± 1
flowing afterglow (300 K)[f]	3.2 ± 20%	26.7			12.0	

[a] Units of 10^{-10} cm^3 s^{-1}. [b] Molecular constants used to calculate capture rates: polarizability, α, obtained from an empirical relation (ref 151); dipole moment, μ_D, obtained experimentally (ref 152); dipole locking constant, $c(T) = 0.227$. Capture rates are calculated at $T = 350$ K. [c] The experimental efficiency, defined as $\Phi_{exp} = k_{obs}(exp)/k_{cap}$, where k_{cap} is determined from the various capture models. [d] Units of kcal mol^{-1}, obtained directly from Figure 5. [e] This work. [f] Reference 17.

Table II. Thermodynamic Data for the Complexation Reaction $ClCH_2CN + Cl^- \rightarrow [ClCH_2CN{\cdot}Cl^-]$

compound	$\Delta G°_{350,rel}$ (kcal mol^{-1})	$\Delta G°_{350,abs}$ (kcal mol^{-1})	$\Delta S°_{350,abs}$ (cal mol^{-1})	$\Delta H°_{350,abs}$ (kcal mol^{-1})	CA = $\Delta H°_{0,abs}$ (kcal mol^{-1})
SO_2	+1.6 ± 0.3	14.7	20.8[a]	20.9	
$ClCH_2CN$	0	13.1 ± 0.3[b] 13.4 ± 0.2[b]	17.7[c]	19.4 ± 0.3	19.6 ± 0.3[d]
CH_3OH	−3.5 ± 0.2	9.9	22.9[a]	16.8	

[a] Entropy estimated using statistical thermodynamic approximations (ref 63). [b] Top and bottom lines corresponds to the absolute free energy change based on the equilibrium measurement relative to SO_2 and CH_3OH, respectively. [c] Entropy calculated from statistical thermodynamic relationships (ref 64) using geometries and frequencies obtained from ab initio calculations at the 6-31+G(d,p) RHF level of theory. [d] Correction to 0 K based on heat capacity calculated from ab initio results at the 6-31+G(d,p) RHF level of theory.

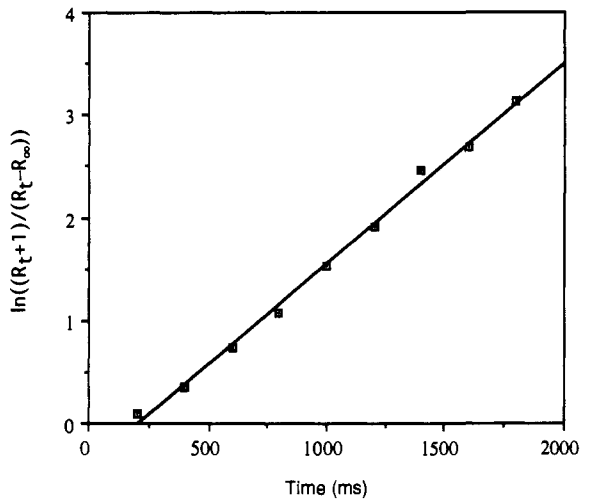

Figure 2. Kinetic data analysis for the representative run given in Figure 1.

obtained from equilibrium measurements relative to known reference compounds, as described above.

$$[ClCH_2CN{\cdot}Cl]^- \rightarrow ClCH_2CN + Cl^- \qquad \Delta H° = CA \qquad (7)$$

For the equilibria established in the thermodynamic studies (eq 8),

$$[ClCH_2CN{\cdot}Cl]^- + CH_3OH \rightleftharpoons ClCH_2CN + [CH_3OH{\cdot}Cl]^- \qquad (8a)$$

$$[ClCH_2CN{\cdot}Cl]^- + SO_2 \rightleftharpoons ClCH_2CN + [SO_2{\cdot}Cl]^- \qquad (8b)$$

standard free energy changes were found using

$$\Delta G°_{rel} = -RT \ln K_{eq} \qquad (9)$$

where "rel" indicates that the reaction involves a relative chloride affinity. Results for the absolute free energy change of eq 7, $\Delta G°_{abs}(ClCH_2CN)$, were then obtained from the corresponding values for CH_3OH and SO_2 determined by Larson and McMahon,[60] whose absolute scale is anchored to the standard free energies of Cl^- complexation of H_2O and *tert*-butyl alcohol at 300 K. As shown in Table II, the values arising from the CH_3OH and SO_2 equilibrium data are internally consistent within 0.3 kcal mol^{-1}. It should be noted that the results presented here were obtained from experiments carried out near 350 K, whereas the results of Larson and McMahon were obtained at 300 K. However, the resulting error in the $\Delta G°_{abs}(ClCH_2CN)$ value is estimated to be only of the order of 0.1 kcal mol^{-1}.

In order to obtain the enthalpy of complexation, $\Delta H°_{abs}(ClCH_2CN)$, from the free energy data, the entropy change, $\Delta S°_{abs}(ClCH_2CN)$, is needed. Larson and McMahon[60,62] have used a statistical thermodynamic approximation in which crude geometry estimates are used and vibrational entropy changes are neglected. Because accurate values for the appropriate parameters of the complex and separated reactants (geometry and vibrational frequencies) have been determined from ab initio computations in this study, all terms (including the vibrational entropy term) were used here in the statistical thermodynamic calculation of the entropy change.[63] The effect of including the vibrational term in evaluating the entropy change is modest but nonnegligible, owing largely to the modes in the complex arising from electrostatic binding. Finally, to facilitate the comparison of experimental and theoretical results, $\Delta H°_{350,abs}$ for chloroacetonitrile is extrapolated to 0 K on the basis of heat capacities ascertained from ab initio data.

The thermodynamic results leading to the chloride affinity of $ClCH_2CN$ are given in Table II. The uncertainties given therein are one standard deviation from the mean of all measurements taken, but the absolute errors are difficult to ascertain and may be somewhat larger. The accuracy in the equilibrium measurements is limited to the accuracy in the relative pressure measurements. This effect probably introduces the largest uncertainty in the final results. Modest uncertainties in the absolute free energy scale and in the computed $\Delta S°_{abs}$ values are also possible. The internal consistency in the relative measurements, however, is encouraging.

C. Discussion of Experimental Results. In this investigation the gas-phase identity exchange reaction of Cl^- with $ClCH_2CN$ (eq 2) is found to have a rate coefficient (3.3×10^{-10} cm^3 s^{-1}) *four* orders of magnitude greater than the value (3.5×10^{-14} cm^3 s^{-1}) for the CH_3Cl/Cl^- system.[15] As seen in Table I, the efficiency of eq 2 corresponds to approximately one substitution event for every 10 collisions, depending on the capture model used. These results are in excellent agreement with the recent findings of DePuy, Bierbaum, and co-workers,[17] who determined rates of identity substitution for a variety of compounds at 300 K, including $ClCH_2CN$, in a flowing afterglow (FA) apparatus. The agreement in the rate measurements is encouraging given that discrepancies in kinetic data obtained from FA and ICR techniques are well documented.[58]

The substitution rate for eq 2 is comparable to the rates of many thermodynamically driven S_N2 reactions, in contrast to most nonhalide identity exchange reactions in which the rates are too slow to be measured.[9] Even in the case of chloride- and bromide-ion identity exchange, there are very few systems reported in the literature that have sufficiently low activation barriers to yield measurable rates.[9,15,17] Qualitatively, these observations suggest that the S_N2 transition state for eq 2 lies below the separated reactants, whereas in most gas-phase S_N2 identity exchange reactions at carbon centers the barrier appears to lie well above the entrance channel. As detailed below in Sections III and IV, both the statistical (μVTST) analysis of the observed reaction rate and the direct ab initio computation of the S_N2 transition state confirm

(62) Larson, J. W.; McMahon, T. B. *J. Am. Chem. Soc.* **1985**, *107*, 766.

(63) McQuarrie, D. A. *Statistical Mechanics*; Harper and Row: New York, 1976.

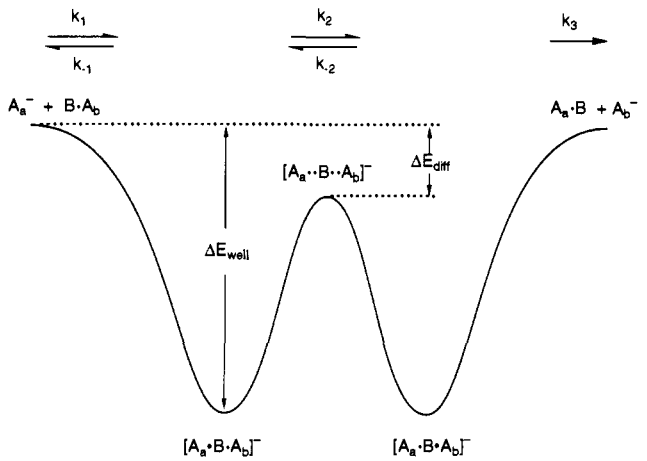

Figure 3. Generalized potential energy surface for a thermoneutral S_N2 identity displacement reaction in the gas phase.

that the activation barrier relative to separated reactants is unusually low for eq 2. A one-dimensional representation of the potential energy surface along the reaction coordinate for the $ClCH_2CN/Cl^-$ system appears in Figure 3, where the S_N2 transition state is shown to be lower in energy than the separated reactants; i.e., $\Delta E_{diff} < 0$. In particular, the value of ΔE_{diff} from the μVTST analysis of the experimental rate is -5.9 ± 1 kcal mol^{-1}, in remarkable agreement with the best ab initio prediction of -6.9 kcal mol^{-1} (vide infra Sections III and IV).

It is clear that an immense rate enhancement for eq 2 relative to the CH_3Cl/Cl^- system is observed due to nitrile substitution at the α carbon, consistent with solution-phase studies. The recent gas-phase results of DePuy, Bierbaum, and co-workers[17] show that other α-substituted alkyl halides involving π systems, including chloroacetone, also exhibit an enhanced reactivity toward identity exchange. An understanding of the electronic structure of these transition states is central to the elucidation of these phenomena, and thus further analysis is reserved for Section IV.

The experimental chloride affinity (CA) determined here for $ClCH_2CN$ is -19.6 kcal mol^{-1} (Table II), a relatively large value which is in excellent agreement with our final ab initio prediction of -18.4 kcal mol^{-1} (see Table XII below). Thus, the ion–molecule complex is ca. 8 kcal mol^{-1} more stable than the corresponding complex for the unsubstituted analogue, $[CH_3Cl\cdot Cl^-]$.[60] Additional comparisons among the chloride-ion binding energies of chloroacetonitrile and numerous other Brønsted acids can be made using the extensive compilation of thermochemical data of Larson and McMahon.[60,64] The $[CH_3F\cdot Cl^-]$ adduct, which represents one extreme, is best viewed as a simple ion–dipole complex in which the 11.5 kcal mol^{-1} binding energy primarily arises from the electrostatic interaction of a negative point charge in the multipole field of the polarizable neutral. At the other extreme is the $[ClHCl]^-$ complex, which exhibits a Cl^- binding energy of 23.1 kcal mol^{-1}. In this case charge transfer is so extensive during adduct formation that the two chlorine atoms become equivalent in the centrosymmetric complex, as substantial relaxation of the molecular orbitals of the system occurs. Representative compounds with intermediate chloride affinities (kcal mol^{-1}, in parentheses) are H_2O (14.4), acetonitrile (15.8), *t*-BuOH (18.1), $CHCl_3$ (18.1), HCN (21.0), and HF (21.8). Compounds of AH type with chloride affinities greater than 23.1 kcal mol^{-1} generally involve neutrals more acidic than HCl and give rise to complexes of $[A\cdot HCl]^-$ character, which are not under consideration here.

Among the cited examples, the chloride-ion binding energy is seen to be correlated with the gas-phase acidity (ΔH_{acid}) of the neutral. Larson and McMahon have investigated this correlation extensively and have found, for example, that a plot of chloride-ion binding energy versus gas-phase acidity for a homologous series of aliphatic alcohols is a straight line with a slope near 0.2. These relationships suggest that the large stability of the $[ClCH_2CN\cdot Cl^-]$ complex is linked to the unusual stability of the conjugate base of $ClCH_2CN$, and hence its acidity. Although the gas-phase acidity of $ClCH_2CN$ is unknown, its value can be bracketed by comparisons with other compounds. Since the proton-transfer reaction of $ClCH_2CN$ with Cl^- leading to the conjugate anion $ClCHCN^-$ was not observed in our experiments, $ClCH_2CN$ must be less acidic than HCl. On the other hand, chloroacetonitrile is expected to be more acidic than CH_3CN as a consequence of additional inductive stabilization of the conjugate anion provided by the electronegative Cl substituent; moreover, CH_3CN itself is relatively acidic because its conjugate anion is stabilized by resonance delocalization of charge into the nitrile moiety. Therefore, the observation of an experimental chloride-ion binding energy of $ClCH_2CN$ which is 3.8 kcal mol^{-1} greater than that of CH_3CN but 3.5 kcal mol^{-1} less than the analogous value for HCl is quite reasonable.

Scheme II

$$AH + A^- \rightarrow [AHA]^- \quad (10a)$$

$$HCl + Cl^- \rightarrow [ClHCl]^- \quad (10b)$$

$$AH + Cl^- \rightarrow [AH\cdot Cl]^- \quad (10c)$$

$$AH + Cl^- \rightarrow A^- + HCl \quad (10d)$$

The correlation of chloride affinity and ΔH_{acid} can be rationalized by invoking Marcus theory applied to proton transfer, as described by Murdoch.[65] The component processes for such an analysis are given in Scheme II. Reactions 10a and 10b involve intrinsic ion-binding energies ΔE_a and ΔE_b, respectively, and reaction 10c involves the chloride affinity of concern, ΔE_c. Moreover, in eq 10d, $\Delta E_d = \Delta H_{acid}(AH) - \Delta H_{acid}(HCl)$ at $T = 0$ K. According to the Marcus theory postulate,[18]

$$\Delta E_c = \frac{1}{2}(\Delta E_a + \Delta E_b) + \frac{1}{2}\Delta E_d + \frac{1}{8}\frac{(\Delta E_d)^2}{(\Delta E_a + \Delta E_b)} \quad (11)$$

Hence, both linear and quadratic terms in ΔH_{acid} appear in eq 11, but, to the degree that the latter are small, a linear correlation is predicted between chloride affinities and gas-phase acidities for homologous compounds.

In comparing F^- and Cl^- binding energies for various series of compounds, Larson and McMahon were led to the conclusion that "chloride binds protic substrates with far more electrostatic character than does fluoride ion". Mulliken population analyses performed here on the $[ClCH_2CN\cdot Cl]^-$ complex (at the RHF level of theory with several basis sets) indicate a net charge of -0.96 on the Cl^- ion. Consistent with the geometric structure (see Section IV), the charge delocalization in the chloride adduct is then quite small, and the binding in the complex is still primarily electrostatic in character even though the chloride affinity is large. In this regard it is worth noting that even the $[FH\cdot Cl]^-$ complex, with a binding energy of 21.8 kcal mol^{-1}, exhibits a localized charge distribution; the excess charge on Cl is ca. -0.92, and the equilibrium bond distances are r(H–F) = 0.96 Å and r(H–Cl) = 1.94 Å, the former distance being only 0.05 Å longer than in HF itself and the latter separation being a full 0.36 Å greater than in $[ClHCl]^-$.[66]

To quantify the various energy contributions to the chloride-ion binding in chloroacetonitrile, a sequence of ab initio calculations[67] was performed according to the following procedure. (1) The RHF electrostatic potential due to the charge distribution of the neutral was determined at the position in space ($\mathbf{R}^-$) that Cl^-

(64) Larson, J. W.; McMahon, T. B. *J. Am. Chem. Soc.* **1984**, *106*, 517.

(65) Murdock, J. R. *J. Am. Chem. Soc.* **1972**, *94*, 4410.

(66) Klepeis, N. E., Masters Thesis, Stanford University, 1991.

(67) All results were obtained with the 6-31+G(d,p) basis set, for which the effect of basis set superposition error (BSSE) is less than 0.15 kcal mol^{-1} at the RHF level. In steps 1 and 2, the 6-31+G(d,p) RHF geometry of the neutral was utilized, as given in Table III. The corresponding position of the Cl^- ion in the complex was found using $r(C_3–Cl_7)$ = 3.3416 Å and $\alpha(Cl_7–C_3–C_2)$ = 119.31° from Table IV (see Figure 6). The complex geometry in step 3 was the optimum C_s-symmetry, RHF structure in Table IV. In step 4, electron correlation was gauged by the MP_∞ extrapolation of the MP4 results at the 6-311+G(d,p) MP2 geometries.

occupies in the complex. (2) A point charge of $-e$ was fixed at $\mathbf{R}^-$, and the RHF energy of the system was computed while allowing the charge distribution of the neutral to polarize. (3) With a chloride ion at $\mathbf{R}^-$, an all-electron RHF calculation was performed after allowing geometry relaxation of the neutral fragment to occur. (4) Dispersion effects were included by incorporating electron correlation into the determination of the binding energy. In step 1 the electrostatic energy of binding arising solely from the preexisting charge distribution of the neutral is found. In step 2 the total electrostatic contribution to the chloride affinity of the neutral is obtained. The results of step 3 give the binding energy including not only interfragment electrostatic interactions, but also interfragment Pauli repulsions of the electrons and contributions due to electronic and geometric rearrangements. Insofar as the level of theory is sufficient in step 4, the resulting value includes all quantum mechanical effects and corresponds to that which is empirically observable.

In steps 1, 2, 3, and 4, the values predicted for the chloride-ion binding energy of $ClCH_2CN$ are 15.76, 19.37, 15.71, and 17.15 kcal mol^{-1}, respectively. Note that the changes arising in steps 2, 3, and 4 are relatively small and even partially offset one another. Therefore, the character of the $[ClCH_2CN{\cdot}Cl]^-$ complex is properly described as electrostatic. For comparison, the sequence of results for CH_3Cl is 8.37, 11.05, 8.96, and 9.66 kcal mol^{-1}, respectively, for steps 1–4.[68] Accordingly, the difference of approximately 8 kcal mol^{-1} between the chloride affinities of chloroacetonitrile and CH_3Cl is accounted for completely by differences in the preexisting charge distributions of the two neutral species. Presumably these variations in electron density distribution are also indicative of the gas-phase acidities of the two compounds, such that the correlation of chloride affinity with ΔH_{acid} embodied in eq 11 is established. In fact, the removal of a proton from a neutral can be decomposed into three steps such that ΔH_{acid} consists of contributions from the following processes: (a) removal of the proton in the fixed electrostatic field which initially exists in the neutral; (b) relaxation of the electron distribution around the center previously occupied by the proton, under the constraint of a fixed geometric structure; (c) and final relaxation of the geometric structure in the conjugate anion. The magnitudes of the contributions from steps a and b are much larger than c. In the case of the CH_3Cl and $ClCH_2CN$ systems, the energy differences for step a are +681 kcal mol^{-1} and +647 kcal mol^{-1}, respectively, at the 6-31+G(d,p) RHF level of theory. Therefore, smaller negative values for the electrostatic potentials (ϕ_{H^+}) at the acidic proton positions in the neutral species seem to correlate with larger positive values (ϕ_{Cl^-}) for the potential at the Cl^- positions in the chloride-ion adducts: CH_3Cl/Cl^-, $e(\phi_{H^+}, \phi_{Cl^-})$ = (−681, +8.4) kcal mol^{-1}; $ClCH_2CN/Cl^-$, $e(\phi_{H^+}, \phi_{Cl^-})$ = (−647, +15.8) kcal mol^{-1}. To the degree that step b enhances or at least does not override the apparent correlation in step a, a physical basis for the ΔH_{acid} versus chloride affinity correlation is established. This issue warrants further study.

III. Statistical Theory of Reaction Rate

A. Methodology. The primary purpose of the statistical analysis presented here is to estimate the S_N2 barrier height from the experimental kinetic data by modeling the efficiency for identity exchange as a function of the activation energy. Part of this analysis involves the modeling of unimolecular dissociation through a "loose" transition state, which is a problem of current research interest. In modeling this process, phase space theory (PST)[36,39,69] and the statistical adiabatic channel model (SACM)[44,70–72] have been used extensively, in addition to several other statistical models involving the transition-state assumption, most of which are based on the well-known RRKM formalism. The latter methods include a nonvariational RRKM model in which a single transition state is chosen to coincide with an average centrifugal barrier,[73] as well as variational models, such as canonical variational transition-state theory (CVTST)[25,74] and its microcanonical analogue (μVTST), which are designed to locate the optimum position of the transition state. Inasmuch as the potential energy surface for the cases of concern increases monotonically in the dissociation channel, the position and number of the microcanonical dynamical transition states depend strongly on both the total energy and the total angular momentum of the system. Moreover, ambiguity can arise in the selection and parameterization of the reaction path implicit in the statistical analysis. Finally, as the dissociation proceeds, problems can arise owing to the uncoupling of modes involving relative rotations of the fragments from vibrational modes which behave adiabatically. These effects can make the implementation of proper statistical treatments difficult. Miller[43] was the first to address many of these dynamical problems in the development of the "unified statistical model", which is useful in the treatment of multiple dynamical bottelnecks in a single reaction channel. In 1985 Wardlaw and Marcus[75–77] developed a variational transition-state approach which addressed the uncoupling of modes problem. In their model the coupled rotational modes, termed transitional modes, are treated separately from the vibrational modes of the individual fragments, which are in turn completely decoupled from the reaction coordinate. In 1990 Smith, Gilbert, and co-workers[32] proposed a similar model for ion–molecule dissociations. These techniques give reasonable results which are qualitatively consistent with one another. However, for our central purpose of extracting the S_N2 barrier height from the observed kinetic data, the effort required to implement the most sophisticated models is not necessary since the calculated value for ΔE_{diff} is only weakly dependent on the choice of the model. In the standard μVTST approach used here, the position of the transition state is determined variationally, and all modes are treated as active.

(a) μVTST Applied to Substitution Reactions in the Gas Phase. As shown in Figure 3, an identity substitution process in the gas phase involves the initial association of A_a^- and BA_b to form a chemically activated, ion–molecule dimer, $[A_a{\cdot}BA_b]^{-\dagger}$ (step 1). This dimer can proceed via substitution to form a second, chemically equivalent dimer, $[A_aB{\cdot}A_b]^{-\dagger}$ (step 2), or it can dissociate to re-form reactants (step −1). If the second complex is formed through substitution, it in turn can either undergo back-substitution to the initial complex (step −2), or it can dissociate to products, $A_aB + A_b^-$ (step 3). The overall rate of reaction for such a system is given by

$$d[A_b^-]/dt = k_{obs}[A_a^-][BA_b] \tag{12}$$

and within the steady-state approximation,

$$k_{obs} = \frac{k_1k_2k_3}{k_{-1}k_{-2} + k_{-1}k_3 + k_2k_3} \tag{13}$$

where the k_i values represent the rate coefficients for the various steps depicted in Figure 3. For a symmetric, thermoneutral reaction, several rate coefficients are equal, and thus

$$k_{obs} = k_1k_2/(2k_2 + k_{-1}) \tag{14}$$

A more convenient representation of the propensity for such a substitution process is the macroscopic efficiency, $\Phi(T)$, which is defined by

(68) These values were also obtained with the 6-31+G(d,p) basis set. In steps 1 and 2, the optimum 6-31+G(d,p) RHF geometry of CH_3Cl was employed: r(C–Cl) = 1.7860 Å, r(C–H) = 1.0782 Å, and α(H–C–Cl) = 108.37°. At the same level of theory, the Cl^- ion in the complex is located 3.3623 Å from the central carbon. In step 3 the relaxed RHF geometry for the CH_3Cl moiety was used: r(C–Cl) = 1.8244 Å, r(C–H) = 1.0738 Å, and α(H–C–Cl) = 107.98°. In step 4 electron correlation was gauged by the MP∞ extrapolation of the MP4 results at the 6-31G(d,p) MP2 geometry of ref 50.

(69) Chesnavich, W. J.; Bowers, M. T. *J. Chem. Phys.* **1977**, *66*, 2306.

(70) Troe, J. *J. Chem. Phys.* **1983**, *79*, 6017.

(71) Troe, J. *Ber. Bunsenges. Phys. Chem.* **1988**, *92*, 242.

(72) Troe, J. *J. Chem. Phys.* **1987**, *87*, 2773.

(73) Waage, E. V.; Rabinovitch, B. S. *Chem. Rev.* **1970**, *70*, 377.

(74) Truhlar, D. G.; Hase, W. L.; Hynes, J. T. *J. Phys. Chem.* **1983**, *87*, 2664; Hase, W. L. *Acc. Chem. Res.* **1983**, *16*, 258.

(75) Wardlaw, D. M.; Marcus, R. A. *J. Chem. Phys.* **1985**, *83*, 3462.

(76) Wardlaw, D. M.; Marcus, R. A. *J. Phys. Chem.* **1986**, *90*, 5383.

(77) Wardlaw, D. M.; Marcus, R. A. *Adv. Phys. Chem.* **1987**, *70*, 231.

$$\Phi(T) = \frac{k_{obs}(T)}{k_1(T)} = \frac{k_2(T)}{2k_2(T) + k_{-1}(T)} \quad (15)$$

The macroscopic efficiency can be represented in terms of its microscopic counterpart for a chemically activated system according to

$$\Phi(T) = \int_0^\infty \int_0^\infty \Phi(E,J)F(E,J;T)\,dE\,dJ \quad (16)$$

where $F(E,J;T)$ represents the distribution of activated complexes initially formed at temperature T with energy E and total angular momentum J. The form of $F(E,J;T)$ is discussed later in this section.

In analogy with eq 15, the microscopic efficiency is determined from microscopic rate coefficients, $k_i(E,J)$, according to:

$$\Phi(E,J) = \frac{k_2(E,J)}{2k_2(E,J) + k_{-1}(E,J)} \quad (17)$$

The individual rate coefficients in eq 17 can be evaluated using unimolecular reaction rate theory. Important contributions from a variety of researchers have lead to the well-known μVTST expression,[23,24,36-45]

$$k(E,J) = \sigma\frac{\int_0^{\epsilon(J;R^*)} \rho^\dagger{}_{\mu VTST}(\epsilon')\,d\epsilon'}{h\rho[\epsilon(J;R_e)]} = \sigma\frac{W^\dagger{}_{\mu VTST}[\epsilon(J;R^*)]}{h\rho[\epsilon(J;R_e)]} \quad (18)$$

where σ is the reaction path degeneracy, R denotes the reaction coordinate, $\epsilon(J;R) = E - V(R) - E_r(J;R)$, $W^\dagger{}_{\mu VTST}[E,J]$ is the number of accessible states at the transition state (located at $R = R^*$) for the (E,J) channel, and $\rho[\epsilon(J;R_e)]$ is the corresponding density of states for the appropriate ion–molecule dimer (for which $R = R_e$). The functions $V(R)$ and $E_r(J;R)$ represent the potential energy and the orbital rotational energy, respectively, along the reaction coordinate, the form of these functions being considered in detail below. For the evaluation of k_{-1}, the location of the (loose) transition state in eq 18 is chosen so that $W^\dagger$ is minimized:[40]

$$W^\dagger{}_{\mu VTST}(E,J) = \min_R\{W^\dagger[\epsilon(J;R)]\} \quad (19)$$

where the minimization is performed over all possible values of R in the entrance channel for each E and J. In the determination of k_2, R^* in eq 18 is selected to coincide with the (tight) S_N2 transition state.

The bimolecular association rate coefficient in eq 15, $k_1(T)$, can be determined by different methods. The standard assumption[24,78] states that $k_1(T)$ is equivalent to the electrostatic capture rate coefficient. Under this assumption, k_1 can be calculated, for example, using average dipole orientation (ADO) theory[79-81] or the parameterized trajectory model of Su–Chesnavich[82] (SC). Alternatively, k_1 can be obtained directly from k_{-1} by microscopic reversibility using the relation,[24]

$$K_{eq} = \frac{k_1(T)}{k_{-1}(T)} = \frac{Q_{AB}}{Q_A Q_B}\exp\left\{\frac{\Delta H^\circ{}_0}{k_B T}\right\} \quad (20)$$

where Q_X represents the partition function of species X, k_B is Boltzmann's constant, and $\Delta H^\circ{}_0$ is the enthalpy of complexation at 0 K. This expression can be used to test the degree to which the μVTST procedure reproduces the expected high-pressure association rate. The results for the capture rates, $k_1(T)$, for the system shown in eq 2, obtained from the three approaches (ADO, SC, and μVTST) are given, for comparison, in Table I.

(b) Conservation of Angular Momentum. The principles involved in the application of eq 18 to ion–molecule systems have been discussed in detail by Gilbert and Smith.[24] The unifying concept for generalized ion–molecule reactions (as represented in eq 21) involves the uncoupling of the orbital angular momentum of the system from the other degrees of freedom for the purpose of enumerating the accessible states along the reaction path.

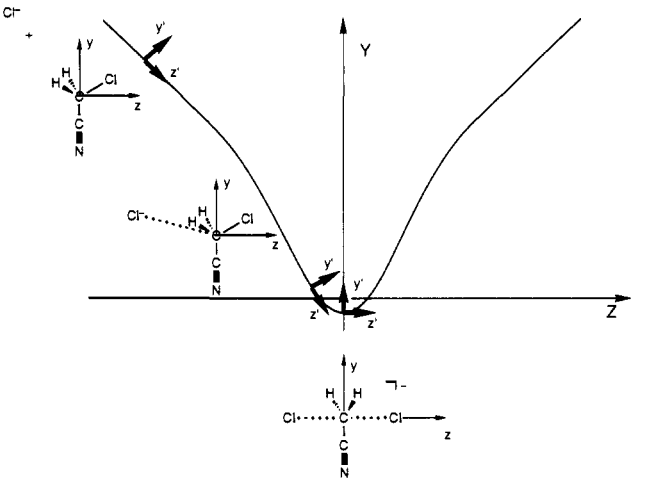

Figure 4. Position of the center-of-mass (Y,Z) in the chloroacetonitrile-fixed axis system for the S_N2 identity reaction of eq 2.

$$A^- + BC \rightarrow [A{\cdot}BC]^- \rightarrow [A{-}B{-}C]^{\dagger-} \rightarrow [AB{\cdot}C]^- \rightarrow AB + C^- \quad (21)$$

In this picture, orbital angular momentum (**L**) is assumed equivalent to total rotational angular momentum (**J**) and is thus conserved as the reaction proceeds. This approximation is particularly suitable to ion–molecule reactions, for which the long-range, electrostatic interaction causes collisions with large impact parameters (and hence large **L**) to predominate in the determination of the thermal rate coefficient. If the A, B, and C subsystems in eq 21 are viewed as atomic fragments interacting in a linear arrangement throughout the reactive encounter, then the approximation **J** = **L** becomes rigorous. The assumption of conservation of orbital angular momentum gives rise to an effective potential for the reactive channel (E,J), viz.

$$V_{eff}(J;R) = V(R) + E_r(J;R) = V(R) + B(R)J(J+1) \quad (22)$$

where $B(R)$ is the effective rotational constant for orbital motion of the reduced system.

(c) Reaction Path for S_N2 Identity Exchange. The dipole moment, μ_D, of chloroacetonitrile is directed at an angle of 156.8° relative to the C_3–C_2 bond vector (Figure 6).[83] While the path of steepest descent from reactants to the complex lies asymptotically along μ_D, the reacting Cl^- must deviate significantly from the dipole vector to effect backside displacement. However, backside approach of Cl^- along the C_3–Cl_6 axis, which is ostensibly ideal for S_N2 substitutions, bypasses the ion–molecule complex structure and leads to a greatly diminished long-range attractive potential, because the dipole moment of chloroacetonitrile is nearly perpendicular to the C_3–Cl_6 bond vector. An appropriate selection of reaction path for eq 2 thus requires an intermediate direction of approach for the chloride ion. *Many choices for this path are reasonable, but the sensitivity of the final value of ΔE_{diff} obtained from the observed rate coefficient appears to be less than 1 kcal mol^{-1} as various paths are invoked.*

In Figure 4 the reaction path chosen here for eq 2 is depicted. By fixing the Cl^- nucleophile at a distance of 10 Å from the center of mass of chloroacetonitrile and by computing 6-31+G(d,p) RHF energy points (see section IV) as a function of the angle of attack, a direction of 130.9° with respect to the C_3–C_2 bond vector is found to be optimal energetically. To aid in the mathematical construction of the corresponding reaction path, the C_3 carbon atom

(78) Chesnavich, W. J.; Bowers, M. T. *Prog. React. Kinet.* **1982**, *11*, 137.
(79) Su, T.; Bowers, M. T. in *Gas Phase Ion Chemistry*; Bowers, M. T., Ed.; Academic Press: New York, 1979; Vol. 1, p 83.
(80) Su, T.; Bowers, M. T. *Int. J. Mass Spectrom. Ion Phys.* **1975**, *17*, 211.
(81) Su, T.; Bowers, M. T. *Int. J. Mass Spectrom. Ion Phys.* **1973**, *12*, 347.
(82) Su, T.; Chesnavich, W. J. *J. Chem. Phys.* **1982**, *76*, 5183.

(83) The 156.8° angle is that predicted at the TZ3P+R+(2f,d) RHF level of theory; the 6-31+G(d,p) RHF wave function provides a value of 153.2°, which shifts steadily upward as the basis set is enlarged.

of the chloroacetonitrile group is placed at the origin of the coordinate system while the carbon atom in the CN substituent lies along the y axis. The Cl atom attached to the central carbon is located in the yz plane. As the reaction is initiated, the center of mass of the entire system is chosen to move in along the asymptote $y = \beta(z - Z_{ClCH_2CN}) + Y_{ClCH_2CN}$, where β = tan (130.9° − 90.0°) and $(Y_{ClCH_2CN}, Z_{ClCH_2CN})$ is the center of mass of the chloroacetonitrile moiety. Upon formation of the ion–molecule complex, the center of mass is positioned at (0, 0.0370, −0.4107) Å, whereas in the S_N2 transition state it is located at (0, −0.3752, 0) Å.[84] A simple expression which correctly reproduces these data for the position (Y, Z) of the center of mass (in Å) along the reaction path is

$$Y(Z) = Y_0 + (1 - e^{-\alpha Z^2})(2 + \sqrt{1 + \beta^2 Z^2}) \qquad (23)$$

where $Y_0 = -0.3752$, $b_0 = 0.6123$, $\alpha = 1.9184$, and $\beta = 0.8656$. The position of the center of mass of the entire system can then be employed to determine the value of R, the separation of the Cl^- ion from the center of mass of chloroacetonitrile. As a global reaction coordinate, R is less appropriate than s, the directed arc length along the $Y(Z)$ curve starting from the origin in Figure 4, but R essentially differs from s only by a constant for $R > 10$ Å. Thus, an R parameterization of the reaction path is utilized in the vicinity of the loose transition states, as determined from[85]

$$R = \frac{M}{m_{Cl}}\sqrt{(Y - Y_{ClCH_2CN})^2 + (Z - Z_{ClCH_2CN})^2} \qquad (24)$$

where M is the total mass, and m_{Cl} denotes the mass of the Cl^- fragment. The direction vector $(1, \partial Y/\partial Z)$ (as determined from eq 23) defines the instantaneous, molecule-fixed, internuclear z' axis, which corresponds to the axis along which the idealized $[A–B–C]^-$ system in eq 21 evolves. The orientation of the z' axis relative to the chloroacetonitrile-fixed system is shown in Figure 4 for selected configurations along the reaction profile.

In applying eq 18 to the reactive system depicted in Figure 4, the geometric mean of the instantaneous moments of inertia about the x' and y' axes provides the effective rotational constant $B(R)$ in eq 22, i.e., $B(R) = \hbar^2/2\sqrt{I_{x'x'}I_{y'y'}}$. Instantaneous rotation about the z' axis, as represented by a free rotor with moment of inertia $I_{z'z'}$, is treated as an internal mode of the system which freely exchanges energy with the set of geniune internal modes. In both the ion–molecule complex and the S_N2 transition state, all of the genuine internal motions are treated as quantized vibrations within the harmonic oscillator approximation. However, in the entrance channel near the loose transition states arising from eq 19, a two-dimensional hindered rotor model is selected for the internal rotations of chloroacetonitrile about the x' and y' axes, the center of mass of the neutral fragment remaining fixed at $(Y_{ClCH_2CN}, Z_{ClCH_2CN})$. The associated rotational barrier is estimated from the magnitude of the dipole moment of the neutral as $2\mu_D e/(4\pi\epsilon_0 R^2)$, and the moment of inertia is taken as the geometric mean of the moments of $ClCH_2CN$ about the x' and y' axes.

A simple (2, 4, 6, 8) analytic form is chosen to model V(R) in the entrance channel:

$$V(R) = -\frac{\mu_D e \cos(25.9°)}{(4\pi\epsilon_0)R^2} - \frac{\alpha e^2}{2(4\pi\epsilon_0)R^4} - \frac{x_a}{R^6} + \frac{x_r}{R^8} \qquad (25)$$

SI units being assumed throughout. The 25.9° angle in eq 25 arises from the orientation of μ_D relative to the direction of Cl^- approach. In addition, α is the polarizability of chloroacetonitrile along the same direction of approach. The constants associated with the r^{-6} attractive and r^{-8} repulsive terms, x_a and x_r, respectively, are selected such that the final ab initio value for ΔE_{well}, the depth of the well in $V(R)$, is reproduced, and the minimum is located at the equilibrium ion–molecule center-of-mass separation, R_e. The pertinent numerical values are $\mu_D = 2.95$ D, $\alpha = 4.69$ Å^3,[86] $R_e = 3.98$ Å,[87] $\Delta E_{well} = 18.4$ kcal mol^{-1}, $x_a = 1.19 \times 10^5$ kcal mol^{-1} Å^6, and $x_r = 1.65 \times 10^6$ kcal mol^{-1} Å^8.

(d) Distribution Function for a Chemically Activated System. The form of the distribution function, $F(E,J;T)$, in eq 16 can be obtained by considering microscopic reversibility between reactants and the associated ion–molecule complex and also by assuming that the colliding species are initially in thermal equilibrium at some temperature, T:[23,34,35,73]

$$F(E,J;T) = \left[(2J+1)W^{\dagger}_{\mu VTST}[E - V_{eff}(J;R^*)] \times \exp\left\{\frac{-(E + V_{eff}(J;R^*))}{k_B T}\right\}\right] \Big/ \left[\int_0^\infty \int_0^\infty (2J+1)W^{\dagger}_{\mu VTST}[E - V_{eff}(J;R^*)] \times \exp\left\{\frac{-(E + V_{eff}(J;R^*))}{k_B T}\right\} dE\, dJ\right] \qquad (26)$$

Verboom and Meisels[34] first derived eq 26 using an analytic Langevin (single-term) potential starting from a Boltzmann distribution of colliding partners and a statistical distribution of impact parameters. It can be shown that the $F(E,J;T)$ distribution is directly related to the population distribution, $P(E,J;T)$, of the ion–molecule complex.[39] Bass et al.[39] have previously noted that these distributions are functions of the rate coefficients for the individual $W^{\dagger}(E,J)$ channels.

(e) Program. The μVTST calculations were performed using the program HYDRA[88] running on a microVAX 3900. The densities and sums of states were determined using the Beyer–Swinehart direct-count algorithm[89] for the vibrational modes and a classical treatment for the internal rotations.[24,90] The subroutine implementing the procedure was taken, with modification, from other RRKM programs written by Bunker and Pattengill[91] and later modified by Gilbert et al.[92,93] Integration was performed numerically with convergence better than one part in 10^4. For each reaction channel, the sum of states was calculated at 20 different center of mass separations (R) of the ion and neutral. To determine the overall minimum in the sum of states along each loose transition state channel, quadratic interpolation about the minimum $W^{\dagger}(E,J)$ point was used.

(f) μVTST Parameters. The data used in the μVTST calculations were obtained from the best ab initio predictions presented in Section IV. The vibrational frequencies for the stationary points along the reaction path were taken from the scaled (SQM) values listed in Tables VIII, IX, and XI. The C_s-symmetry complex shown in Figure 6, which is that traversed by the reaction path, is actually not a local minimum on the potential energy surface,

(84) In Tables IV and V, geometric parameters are listed at the 6-311+G(d,p) MP2 level for the $ClCH_2CN \cdot Cl^-$ complex and the S_N2 transition state, respectively. These data were utilized to determine the quoted center-of-mass positions, except that substitutions from the TZ3P+R+(2f,d) MP2 results for the $r(C_3–Cl_7)$ distances were made (see footnote *b* of Tables IV and V).

(85) This parameterization is only necessary in the entrance channel, where eq 19 is applied to locate the loose, variational transition states. At the 6-311+G(d,p) MP2 level of theory, the value of $(Y_{ClCH_2CN}, Z_{ClCH_2CN})$ only varies from (−0.4141, +0.7523) Å to (−0.4337, +0.7674) Å in going from the neutral to the ion-molecule complex. Thus, $Y_{ClCH_2CN} = -0.4141$ and $Z_{ClCH_2CN} = 0.7523$ are employed as fixed values in eq 23.

(86) Computed at the 6-31+G(d,p) RHF level of theory, in good agreement with a spherically-averaged polarizability of 6.32 Å^3 determined from an empirical relation (ref 155).

(87) R_e extracted from eq 23.

(88) Wladkowski, B. D.; Lim, K. F.; Brauman, J. I. **1991**, Program HYDRA: details available upon request.

(89) Beyer, T.; Swinehart, D. F. *Commun. Assoc. Comput. Machin.* **1973**, *16*, 379.

(90) Zare, R. N. *Angular Momentum*; Wiley-Interscience: New York, 1988.

(91) Bunker, D. L.; Pattengill, M. *J. Chem. Phys.* **1968**, *48*, 772. Hase, W. H.; Bunker, D. L. *QCPE* **1973**, *11*, 234.

(92) Greenhill, P. G.; Smith, S. C.; Pitt, I. G.; Gilbert, R. G. Program GEOM, **1989**.

(93) Gilbert, R. G.; Jordan, M. J. T.; Smith, S. C. Program package UNIMOL, **1990**.

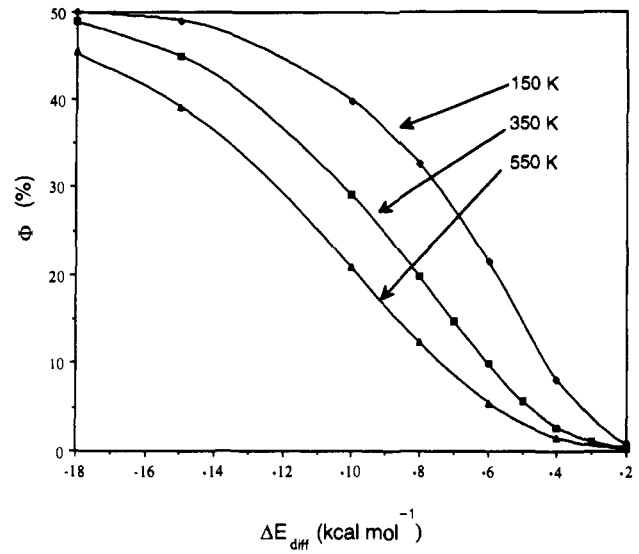

Figure 5. Plot of the μVTST–RRKM efficiency (Φ) vs ΔE_{diff} for the S_N2 identity reaction of eq 2. The points represent calculated efficiencies through which the interpolated curves are drawn.

because the energy profile for the Cl^- out-of-plane torsional mode is a double well with a barrier height of ca. 0.2 kcal mol^{-1} (see Section IV). For vibrational energies substantially above this barrier, the double-well potential can be reasonably replaced by a broad parabola which supports energy-level spacings of $\nu^* = 8^{-1/2}\nu_0$, where ν_0 is equal to the value of ν_{15} in Table X for the C_1-symmetry, hydrogen-bonded complex.[94] Hence, for the purposes of enumerating states for the Cl^- out-of-plane torsional mode of the ion–molecule complex, a frequency of 17 cm^{-1} was employed.

The effective rotational constants $B(R)$ in eq 22 for the external, inactive rotations of the ion–molecule complex and the S_N2 transition state were found to be 0.042 60 cm^{-1} and 0.070 76 cm^{-1}, respectively, according to the scheme described above. For $R >$ 10 Å, where most loose transition states reside, the corresponding $B(R)$ values lie close to those predicted from an effective moment of inertia equal to $m_{Cl}m_{ClCH_2CN}/(m_{Cl} + m_{ClCH_2CN})R^2$. For the active, external rotational constant associated with $I_{z'z'}$ in Figure 4, values of 0.063 20 cm^{-1} and 0.043 32 cm^{-1} were found for the complex and the tight transition state, respectively. For the loose transition states, this constant remains close to 0.1058 cm^{-1} over the pertinent region $R >$ 10 Å. Finally, in the entrance channel the mean rotational constant for the hindered rotations of chloroacetonitrile about the x' and y' axes does not vary significantly from its 0.2335-cm^{-1} asymptotic value.

B. Statistical Results. The μVTST formalism was used to calculate the efficiency of the reaction in eq 2 as a function of the assumed height of the S_N2 transition state (ΔE_{diff} in Figure 3). The efficiency versus ΔE_{diff} curves for three different temperatures are presented in Figure 5. To extract a value for ΔE_{diff}, the observed rate constant in eq 14 at T = 350 K must be converted into an experimental efficiency using the association rate $k_1(T)$. As seen in Table I, the association rate obtained from eq 20 at 350 K is approximately 50% larger than the values determined from the electrostatic capture models, which are known from experiment and trajectory calculations to reproduce ion–molecule capture rates reasonably well. This overestimation is related to the transitional mode coupling problem discussed above and outlined by Smith, Gilbert, and co-workers.[32] The efficiency at 350 K derived from k_{obs} using the μVTST capture rate to maintain internal consistency is 7.6%, which corresponds to ΔE_{diff} = −5.9 kcal mol^{-1} according to the graph in Figure 5. If the ADO result for $k_1(T)$ is assumed, an efficiency of 14.2% is obtained, which may be closer to the actual value. In this case ΔE_{diff} shifts to −6.8 kcal mol^{-1}. In brief, a final value of $\Delta E_{diff} = -5.9 \pm 1$ kcal mol^{-1} is apparent. It must be emphasized that the error associated with estimating the S_N2 barrier height using the various simplified models is small, 1 kcal mol^{-1} or less. Consequently, we are confident that the errors introduced by the approximations used here still allow the accurate determination of activation energies for a variety of S_N2 systems.

C. Discussion of Statistical Results. The value of ΔE_{diff} (−5.9 kcal mol^{-1}) which reproduces the observed rate for eq 2 at 350 K, as determined via the application of μVTST theory, is in excellent agreement with the final ab initio prediction of −6.9 kcal mol^{-1} reported below (see Section IV). Moreover, if the ab initio value of ΔE_{diff} is used in the μVTST analysis, k_{obs} is found to be 6.1×10^{-10} cm^3 s^{-1}, i.e., within a factor of 2 of experiment. If this level of agreement is maintained for general S_N2 identity exchange reactions, then the application of statistical theory to ascertain ΔE_{diff} from observed rate coefficients (or vice versa) would prove to be a powerful technique. While the level of agreement seen here is very encouraging, it is not clear to what extent errors arising from the assumptions inherent in the statistical analysis fortuitously cancel.

In the past, there have been only a few studies of S_N2 reactions in which the results from ab initio theory and experiment were compared with the aid of statistical theory. Zahradník and co-workers[33] analyzed the substitution process of hydride ion with methyl fluoride ($CH_3F + H^- \rightarrow CH_4 + F^-$) in some detail. Two different RRKM models were used in the study, and ab initio quantum chemical calculations were used to supply the input data for the analyses. The first model is the same as that used previously by Brauman and co-workers.[8-10] In particular, the critical configuration for the loose transition state is located at the top of the centrifugal barrier for some average rotational energy, as described by Waage and Rabinovitch,[73] and the transitional modes are treated as free rotors. In the second model the critical configuration is located at the position of the minimum number of states as given by transition-state theory (TST). The transitional modes are then treated as quantized vibrations, the frequencies of which exponentially decrease as a function of ion–neutral separation. For both models Zahradník and co-workers found modest agreement (within an order of magnitude) between the rate of reaction predicted by RRKM theory and the experimental rate.

The S_N2 reaction of $CH_3Cl + Cl^-$ (eq 1) is the only identity exchange S_N2 reaction where statistical theory has been used in conjunction with ab initio investigations. Tucker and Truhlar performed the first of these studies,[50] in which simple TST was applied. Ab initio data were used to obtain the various partition functions, and agreement within approximately an order of magnitude of the experimental rate obtained by Bierbaum and co-workers[15] was found. More recently, Vande Linde and Hase[49] used a more sophisticated application of TST, viz. canonical variational transition-state theory (CVTST), to model eq 1. First, an analytic representation of the potential energy surface was constructed using ab initio quantum chemical results (6-31G* RHF). The analytic surface was then used to locate the CVTST transition state, where the thermal rate coefficient is a minimum. Two different models were used for the transitional modes for association of Cl^- with CH_3Cl, specifically a two-dimensional classical hindered rotor treatment and a classical harmonic oscillator treatment. The two different models gave similar results and reproduced the experimental rate to within a factor of 2.

In a series of studies Vande Linde and Hase also used their analytic representation of the potential energy surface for eq 1 to perform classical trajectory calculations.[54-56,95,96] A variety of issues were considered, including the effects of mode-selective vibrational excitation, energy randomization during association, energy dependences of the component processes, and multiple

(94) For a one-dimensional, double-well potential $V(x)$ with minima at $x = \pm a$ and a central barrier of height b, $4b/a^2 \approx \kappa\nu_0^2$, where ν_0 is the frequency for harmonic vibrations within one of the wells and κ involves the reduced mass. An enveloping parabola centered at $(x, y) = (0, -b)$ which rises to $y = +b$ at $x = \pm 2a$, then yields energy level spacings of $\nu^* = 8^{-1/2}\nu_0$.

(95) Vande Linde, S. R.; Hase, W. L. *J. Chem. Phys.*, in press.
(96) Cho, Y. J.; Vande Linde, S. R.; Hase, W. L. In preparation.

recrossings of the S_N2 barrier. In the first of these trajectory studies, it was confirmed that substitution events at thermal energies are very improbable. However, selective excitation of the C–Cl stretch (ν_3) in CH_3Cl caused a dramatic increase in the number of substitution events. Most of the substitutions which occurred in this fashion were described as direct substitution events in which "the reactive system is not temporarily trapped in either the minima for the $Cl^-...CH_3Cl$ or $ClCH_3...Cl^-$ ion–dipole complex".[55] At this point inconsistencies with the assumptions of statistical theory became apparent as trajectory calculations revealed that both the energy dependence and the average lifetime of the dissociation process are distinctly non-RRKM. It appears that only certain modes are involved in intramolecular vibrational energy redistribution. In more recent work on eq 1, Vande Linde and Hase showed that a significant number of trajectories initiated at the S_N2 barrier eventually cross it numerous times before dissociating, even though the barrier in the analysis is located well above the reactants (3.8 kcal mol^{-1}).[54,96] The authors conclude that certain modes are strongly decoupled from others along the reaction path and are not available for complete internal vibrational energy randomization.

The implications of the findings of Vande Linde and Hase are far reaching when considering the applicability of RRKM-type theories to S_N2 reactions in the gas phase in that the basic assumptions of the theory are brought into question, especially if the trajectory results on eq 1 can be generalized to other S_N2 systems. However, several central issues are still unresolved. These findings may be specific to relatively simple systems with few oscillators such as the CH_3Cl/Cl^- reaction or only to S_N2 reactions with a high central barrier. Also, the level of theory (6-31G* RHF) used to construct the analytic surface for eq 1 is modest. The potential may adequately describe the essential energetic features[14,49-53] and the intricate coupling of the normal modes, but this is not yet clear.

One difficulty in classical trajectory analyses of systems such as eq 1 is that very few substitution events occur at room temperature. Therefore, the reaction rate and corresponding reaction efficiency cannot be determined accurately via trajectory calculations, as was pointed out by Vande Linde and Hase.[54] It may be that non-RRKM effects observed in specific trajectories have little effect (or a cancelling effect) on the overall theoretical rate of reaction, especially at low energies. We propose that the $ClCH_2CN$ identity exchange reaction is an excellent candidate for trajectory studies which focus on this issue. Even though an analytic potential surface for this reaction does not yet exist, the ab initio results presented in this paper represent a first step toward this goal. Since the barrier is well below the separated reactants, an accurate value of the efficiency could be obtained from classical trajectories and compared directly with experiment. It would be worthwhile to determine whether the non-RRKM behavior observed in the CH_3Cl/Cl^- system is also found in other S_N2 identity systems.

Recently, the applicability of statistical theories to model exothermic S_N2 reactions has received some attention. In particular, the reaction, $Cl^- + CH_3Br \rightarrow CH_3Cl + Br^-$ has been studied by Viggiano and co-workers,[97] who observed nonstatistical kinetics, while in a separate experiment Graul and Bowers[98] have observed a nonstatistical energy distribution for the products of this reaction.

IV. Ab Initio Theoretical Investigation

A. Methods. The salient features of the potential energy surface for the thermoneutral S_N2 identity exchange reaction of chloroacetonitrile ($ClCH_2CN$) with chloride ion (Cl^-), eq 2, were investigated at various levels of electronic structure theory. The features of the surface under investigation included the separated reactants, the S_N2 backside ion–molecule complex (C_s symmetry), the hydrogen-bonded ion–molecule complex (C_1 symmetry), and the S_N2 transition state (C_{2v} symmetry). Most results, including all geometry optimizations and quadratic force field determinations, were obtained using the Gaussian suite of programs;[99] the remaining data analyses, including normal coordinate analyses and scaling of the quantum mechanical force fields, were completed using the INTDER[100] program.

(a) Basis Sets. A variety of basis sets due to Pople and coworkers were used in this study, these sets being designated 3-21G,[101-103] 6-31G,[104-106] 6-31+G,[104-107] 6-31+G(d,p),[104-107] 6-311+G(d,p),[107-109] and 6-311+G(2d,2p).[107-109] The (+) in these particular designations indicates the addition of a set of s- and p-type diffuse functions on all heavy atoms.[107] The sets of polarization functions added to each heavy atom and hydrogen atom are listed sequentially in parentheses. For $[Cl_2CH_2CN]^-$ the 3-21G, 6-31G, 6-31+G, 6-31+G(d,p), 6-311+G(d,p), and 6-311+G(2d,2p) basis sets consist of 57, 57, 77, 113, 138, and 169 contracted Gaussian functions, respectively.

More flexible and highly polarized basis sets of at least valence triple-ζ (TZ) quality were also used in this investigation, these being designated TZ2P+R+f and TZ3P+R+(2f,d). The TZ core for both of these sets is comprised of the McLean-Chandler[109] (12s9p/6s5p) contraction for Cl, the Huzinaga–Dunning[110,111] (10s6p/5s4p) contraction for C and N, and a (6s/4s) contraction from Huzinaga[111,112] for H. Sets of diffuse s and p functions (denoted by R for Rydberg) were then added in an even-tempered sense to all heavy atoms. The corresponding orbital exponents were $\alpha_s(Cl) = 0.06962$, $\alpha_p(Cl) = 0.04365$, $\alpha_s(C) = 0.04561$, $\alpha_p(C) = 0.03344$, $\alpha_s(N) = 0.06376$, and $\alpha_p(N) = 0.04861$. In the TZ2P+R+f basis, two sets of d-type and one set of f-type polarization functions were appended to the heavy atoms with correlation-optimized exponents:[113-115] $\alpha_d(Cl) = 1.072, 0.357$; $\alpha_f(Cl) = 0.700$; $\alpha_d(C) = 1.097, 0.318$; $\alpha_f(C) = 0.761$; $\alpha_d(N) = 1.654, 0.469$; and $\alpha_f(N) = 1.093$. For hydrogen, the TZ2P+R+f basis contains two sets of p-type polarization functions:[113] $\alpha_p(H) = 1.407, 0.388$. The TZ3P+R+(2f,d) basis was constructed similarly using polarization functions of various types with correlation-optimized exponents:[113-115] $\alpha_d(Cl) = 1.8570, 0.6190, 0.2060$; $\alpha_f(Cl) = 1.2124, 0.4042$; $\alpha_d(C) = 1.848, 0.649, 0.228$; $\alpha_f(C) = 1.419, 0.485$; $\alpha_d(N) = 2.837, 0.968, 0.335$; $\alpha_f(N) = 2.027, 0.685$. For hydrogen, however, the same TZ2P+R basis was used with the addition of a single d-function, $\alpha_d(H) = 1.057$. Note that for both basis sets the polarization function exponents for Cl were constructed from reference values of $\alpha_d(Cl) = 0.619$[115] and $\alpha_f(Cl) = 0.700$[114] by using a geometric ratio of 3 in a even-tempered scheme. In both the TZ2P+R+f and TZ3P+R+(2f,d) basis sets, the d and f sets were comprised of five and seven components, respectively, i.e., of true spherical harmonics. The final contraction scheme for the TZ3P+R+(2f,d) basis can be

(97) Viggiano, A. A.; Morris, R. A.; Paschkewitz, J. S.; Paulson, J. F. *J. Am. Chem. Soc.* Submitted for publication.
(98) Graul, S. T.; Bowers, M. T. *J. Am. Chem. Soc.* **1991**, *113*, 9696.

(99) Frisch, M. J.; Head-Gordon, M.; Trucks, G. W.; Foresman, J. B.; Schlegel, H. B.; Raghavachari, K.; Robb, M. A.; Binkley, J. S.; Gonzalez, C.; Defrees, D. J.; Fox, D. J.; Whiteside, R. A.; Seeger, R.; Melius, C. F.; Baker, J.; Martin, R. L.; Kahn, L. R.; Stewart, J. J. P.; Topiol, S.; Pople, J. A. GAUSSIAN 90, Gaussian, Inc.: Pittsburgh PA, 1990.
(100) Allen, W. D. Program INTDER: details available upon request.
(101) Binkley, J. S.; Pople, J. A.; Hehre, W. J. *J. Am. Chem. Soc.* **1980**, *102*, 939.
(102) Gordon, M. S.; Binkley, J. S.; Pople, J. A.; Pietro, W. J., P.; Hehre, W. J. *J. Am. Chem. Soc.* **1982**, *104*, 2797.
(103) Pietro, W. J.; Francl, M. M.; Hehre, W. J.; Defrees, D. J.; Pople, J. A.; Binkley, J. S. *J. Am. Chem. Soc.* **1982**, *104*, 5093.
(104) Hehre, W. J.; Ditchfield, R.; Pople, J. A. *J. Chem. Phys.* **1972**, *56*, 2257.
(105) Hariharan, P. C.; Pople, J. A. *Theor. Chim. Acta* **1973**, *28*, 213.
(106) Gordon, M. A. *Chem. Phys. Lett.* **1980**, *76*, 163.
(107) Clark, T.; Chandrasekhar, J.; Spitznagel, G. W.; Schleyer, P. v. R. *J. Comput. Chem.* **1983**, *4*, 294.
(108) Krishnan, R.; Binkley, J. S.; Seeger, R.; Pople, J. A. *J. Chem. Phys.* **1980**, *72*, 650.
(109) McLean, A. D.; Chandler, G. S. *J. Chem. Phys.* **1980**, *72*, 5639.
(110) Dunning, T. H., Jr. *J. Chem. Phys.* **1971**, *55*, 716.
(111) Huzinaga, S. *J. Chem. Phys.* **1965**, *42*, 1293.
(112) Allen, W. D.; Schaefer, H. F., III *Chem. Phys.* **1986**, *108*, 243.
(113) Dunning, T. H., Jr. *J. Chem. Phys.* **1989**, *90*, 1007.
(114) Ahlrichs, R.; Taylor, P. R. *J. Chim. Phys.* **1981**, *78*, 315.
(115) Frisch, M. J.; Pople, J. A.; Binkley, J. S. *J. Chem. Phys.* **1984**, *80*, 3265.

Table III. Geometric Structure of Chloroacetonitrile[a]

level of theory	RHF 6-31G	RHF 6-31+G	RHF 6-31+G(d,p)	RHF 6-311+G(d,p)	RHF 6-311+G(2d,2p)	MP2 6-311+G(d,p)	experiment[b]
coordinates							
$r(C_2-N_1)$	1.1451	1.1447	1.1344	1.1283	1.1255	1.1747	1.158
$r(C_2-C_3)$	1.4481	1.4499	1.4668	1.4638	1.4635	1.4611	1.472
$r(C_3-H_{4,5})$	1.0751	1.0750	1.0785	1.0781	1.0751	1.0902	1.070 (1.088)[c]
$r(C_3-Cl_6)$	1.8595	1.8588	1.7788	1.7804	1.7823	1.7784	1.767 (1.782)[c]
$\alpha(C_3-C_2-N_1)$	179.09	178.84	178.40	178.36	178.37	178.37	
$\alpha(H_{4,5}-C_3-C_2)$	111.26	111.13	109.42	109.50	109.67	109.41	
$\alpha(Cl_6-C_3-C_2)$	111.41	111.23	111.83	111.65	111.51	111.37	111.24 (111.29)[c]
$\alpha(H_{4,5}-C_3-Cl_6)$	106.04	106.16	108.20	108.21	108.01	108.53	
$\tau(Cl_6-C_3-C_2-N_1)$	180.00	180.00	180.00	180.00	180.00	180.00	
dipole moment	3.47	3.57	3.51	3.49	3.52		2.95[d]

[a] Bond distances in Å, angles in degrees. See Figure 6 for structural depictions. [b] Reference 131. [c] Reference 138. [d] Reference 152.

Table IV. Geometric Structure[a] of the Chloroacetonitrile/Cl^- Complex [$ClCH_2CN\cdot Cl^-$]

level of theory symmetry	RHF 6-31G C_s	RHF 6-31+G C_s	RHF 6-31+G(d,p) C_s	RHF 6-31+G(d,p) C_1	RHF 6-311+G(d,p) C_s	RHF 6-311+G(2d,2p) C_s	MP2 6-311+G(d,p) C_s
coordinates							
$r(C_2-N_1)$	1.1462	1.1460	1.1358	1.1360	1.1298	1.1270	1.1755
$r(C_2-C_3)$	1.4484	1.4507	1.4681	1.4678	1.4650	1.4646	1.4596
$r(C_3-H_{4,5})$	1.0712	1.0721	1.0758	1.0833 (H_4) 1.0770 (H_5)	1.0753	1.0725	1.0876
$r(C_3-Cl_6)$	1.8983	1.8890	1.7970	1.7946	1.7988	1.8009	1.7963
$r(C_3-Cl_7)$	3.1793	3.2954	3.3416	3.4077	3.3440	3.3230	3.1604[b]
$\alpha(C_3-C_2-N_1)$	179.30	178.98	179.76	179.14	179.74	179.40	178.08
$\alpha(H_{4,5}-C_3-C_2)$	112.93	112.83	111.04	111.82 (H_4) 109.58 (H_5)	111.06	111.18	110.73
$\alpha(Cl_6-C_3-C_2)$	108.85	108.80	109.67	109.94	109.59	109.51	109.64
$\alpha(Cl_7-C_3-C_2)$	107.16	114.29	119.31	118.42	119.08	119.42	109.60
$\tau(H_{4,5}-C_3-C_2-N_1)$	105.59	106.67	108.89	109.61 (H_4) 107.64 (H_5)	108.84	108.75	109.69
$\tau(Cl_6-C_3-C_2-N_1)$	0.00	180.00	0.00	107.23	0.00	0.00	0.00
$\tau(Cl_7-C_3-C_2-Cl_6)$	180.00	180.00	180.00	145.44	180.00	180.00	180.00

[a] Bond distances in Å, angles in degrees. See Figure 6 for structural depictions. [b] A reoptimization of this coordinate at the TZ3P+R+(2f,d) MP2 level yielded 3.118 Å (see text).

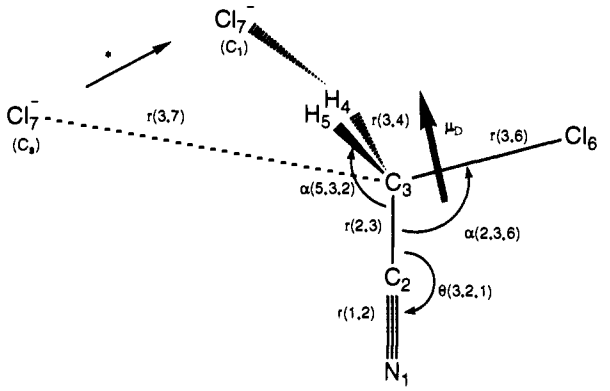

Figure 6. Geometric structure and coordinate descriptions for [$ClCH_2CN\cdot Cl^-$] complexes. The dipole moment vector μ_D of the chloroacetonitrile moiety is shown emanating from the center of mass of the neutral fragment. The movement of the Cl_7^- ion in going from the C_s-symmetry, ion–dipole complex to the C_1-symmetry, hydrogen-bonded complex is depicted by the starred arrow.

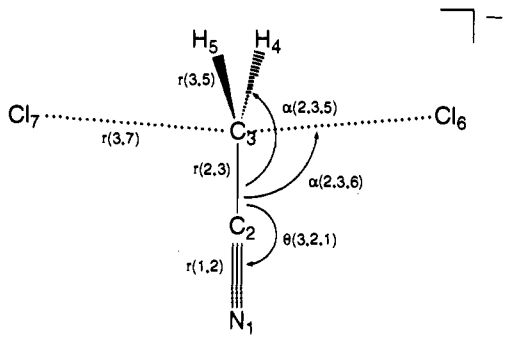

Figure 7. Geometric structure and coordinate descriptions for the S_N2 transition state [$Cl_2CH_2CN^-$].

designated as Cl(13s10p3d2f/7s6p3d2f), C,N(11s7p3d2f/6s5p3d2f), and H(6s3p1d/4s3p1d). For [Cl_2CH_2CN]$^-$ the TZ2P+R+f and the TZ3P+R+(2f,d) basis sets consist of 218 and 289 contracted Gaussian functions, respectively.

(b) Electronic Wave Functions. For all points investigated on the potential surface of interest, electronic wave functions within the restricted Hartree–Fock, self-consistent-field (RHF SCF) approximation were determined. To investigate the effects of electron correlation, Møller–Plesset (MP) perturbation theory,[116-119] including MP2, MP3, and MP4(SDTQ), was used. In some cases the exact non-relativistic energy (MP_∞) within the given one-particle basis set was estimated by extrapolating the MP series using a formula suggested by Pople and co-workers.[120,121] All core orbitals were frozen in the correlation treatments (viz., the 1s orbitals for first-row atoms and the 1s, 2s, and 2p orbitals for the Cl atoms). In contrast, all virtual orbitals were included in the determination of the MPn energies.

(c) Analytic Derivatives and Geometric Structures. The determinations of RHF geometric structures, quadratic force constants, harmonic vibrational frequencies, and infrared and Raman intensities were made viable by the use of analytic derivative

(116) Møller, C.; Plesset, M. S. *Phys. Rev.* **1934**, *46*, 618.

(117) Pople, J. A.; Seeger, R.; Krishnan, R. *Int. J. Quantum Chem. Symp.* **1977**, *11*, 149.

(118) Krishnan, R.; Pople, J. A. *Int. J. Quantum Chem.* **1978**, *14*, 91.

(119) Krishnan, R.; Frisch, M. J.; Pople, J. A. *J. Chem. Phys.* **1980**, *72*, 4244.

(120) Handy, N. C.; Knowles, P. J. *Theor. Chim. Acta* **1985**, *68*, 87.

(121) Pople, J. A. *Int. J. Quantum Chem. Symp.* **1983**, *17*, 307.

Table V. Geometric Structure[a] of Chloroacetonitrile/Cl^- S_N2 Transition State $[Cl_2CH_2CN^-]$ in C_{2v} Symmetry

level of theory	RHF 6-31G	RHF 6-31+G	RHF 6-31+G(d,p)	RHF 6-311+G(d,p)	RHF 6-311+G(2d,2p)	MP2 6-311+G(d,p)
coordinates						
$r(C_2-N_1)$	1.1457	1.1451	1.1350	1.1288	1.1261	1.1781
$r(C_3-C_2)$	1.4327	1.4336	1.4472	1.4448	1.4452	1.4365
$r(C_3-H_{4,5})$	1.0596	1.0598	1.0602	1.0596	1.0565	1.0727
$r(C_3-Cl_{6,7})$	2.4079	2.4141	2.3659	2.3627	2.3503	2.2943[b]
$\alpha(C_3-C_2-N_1)$	180.00	180.00	180.00	180.00	180.00	180.00
$\alpha(H_{4,5}-C_3-C_2)$	119.73	119.61	119.15	119.08	119.17	119.09
$\alpha(Cl_{6,7}-C_3-C_2)$	96.70	96.60	95.94	95.87	95.62	94.16
$\alpha(H_{4,5}-C_3-Cl_6)$	90.00	90.00	90.00	90.00	90.00	90.00

[a] Bond distances in Å, angles in degrees. See Figure 7 for a structural depiction. [b] A reoptimization of this coordinate at the TZ3P+R+(2f,d) MP2 level yielded 2.274 Å (see text).

Table VI. Scale Factors Obtained from SQM Analysis of $ClCH_2CN$ along with Corresponding Symmetry Coordinate Groupings[a]

scale factors	internal modes[b] for $ClCH_2CN$	internal modes[b] for $[ClCH_2CN\cdot Cl^-]$	internal modes[b] for $[Cl_2CH_2CN]^{-\dagger}$
0.7371 (0.0091)	S_1	S_1	S_1
0.8681 (0.0190)	S_2	S_2	S_2
0.8135 (0.0053)	(S_3, S_4)	(S_3, S_4)	(S_3, S_4)
0.7891 (0.0298)	S_5	S_5	S_5
0.9877 (0.0738)	S_6	S_7	(S_7, S_8)
0.7902 (0.0062)	(S_7, S_8, S_9, S_{10})	(S_9, S_{10}, S_{11}, S_{12})	(S_9, S_{10}, S_{11}, S_{12})
0.7744 (0.0215)	(S_{11}, S_{12})	(S_{13}, S_{14})	(S_{13}, S_{14})
1.00[c]		(S_6, S_8, S_{15})	(S_6, S_{15})

[a] The rms error in the SQM fit to the fundamental frequencies of $ClCH_2CN$ is only 5.5 cm^{-1}, and the standard errors for the scale factors (listed in parentheses) are quite small. The magnitudes of all scale factors except that for S_6 are as expected from the propensity of Hartree–Fock theory to provide harmonic vibrational frequencies 10–15% larger than experimental fundamentals. The factor for S_6 is not as well determined by the fit as the rest, and its relatively large value appears to arise from the strong coupling of S_6 to other coordinates in the normal modes of $ClCH_2CN$ (see Table VIII below). [b] Definitions for the various symmetry internal coordinates S_i are given in Table VII. [c] Force constants for the listed coordinates were left unscaled.

Table VII. Definition of Internal Coordinate Sets (S_i) for Chloroacetonitrile and Its Ion–Molecule Intermediates[a]

internal coordinates	description	$ClCH_2CN$	$[ClCH_2CN\cdot Cl^-]$	$[Cl_2CH_2CN^-]^{\dagger}$	symmetry[b]
$r(1,2)$	C≡N stretch	S_1	S_1	S_1	$a'(a_1)$
$r(2,3)$	C—C stretch	S_2	S_2	S_2	$a'(a_1)$
$2^{-1/2}[r(3,4) + r(3,5)]$	CH_2 sym stretch	S_3	S_3	S_3	$a'(a_1)$
$2^{-1/2}[r(3,4) - r(3,5)]$	CH_2 antisym stretch	S_4	S_4	S_4	$a''(b_1)$
$r(3,6)$	C—Cl stretch	S_5	S_5	$2^{-1/2}(S_5 + S_6)$	$a'(a_1)$
$r(3,7)$	C—Cl stretch		S_6	$2^{-1/2}(S_5 - S_6)$	$a'(b_2)$
$\alpha(6,3,2)$	C—C—Cl bend	S_6	S_7	$2^{-1/2}(S_7 + S_8)$	$a'(a_1)$
$\alpha(7,3,2)$	C—C—Cl bend		S_8	$2^{-1/2}(S_7 - S_8)$	$a'(b_2)$
$2^{-1/2}[\alpha(4,3,2) + \alpha(5,3,2)]$	CH_2 deformation[c]	S_7	S_9	S_9	$a'(a_1)$
$2^{-1/2}[\alpha(4,3,2) - \alpha(5,3,2)]$	CH_2 deformation[c]	S_8	S_{10}	S_{10}	$a''(b_1)$
$2^{-1/2}[\alpha(6,3,4) + \alpha(6,3,5)]$	CH_2 deformation[c]	S_9	S_{11}	S_{11}	$a'(b_2)$
$2^{-1/2}[\alpha(6,3,4) - \alpha(6,3,5)]$	CH_2 deformation[c]	S_{10}	S_{12}	S_{12}	$a''(a_2)$
$\theta_a(1,2,3)$	C—C≡N in-plane bend[d]	S_{11}	S_{13}	S_{13}	$a'(b_2)$
$\theta_b(1,2,3)$	C—C≡N out-of-plane bend[d]	S_{12}	S_{14}	S_{14}	$a''(b_1)$
$\tau(7,3,2,6)$	Cl–C–C–Cl torsion		S_{15}	S_{15}	$a''(b_1)$

[a] Numbering of atoms is shown in Figures 6 and 7. $r(i,j)$ = i–j bond distance, $\alpha(i,j,k)$ = i–j–k bond angle, $\theta(i,j,k)$ = linear bending angle of i–j–k chain, $\tau(i,j,k,l)$ = dihedral angle between ijk and jkl planes. [b] The irreducible representations for the C_s-symmetry reactant and ion–molecule complex are listed with the corresponding symmetry types for the S_N2 transition state in parentheses. [c] In the S_N2 transition state, S_9, S_{10}, S_{11}, and S_{12} describe the CH_2 scissor, twist, wag, and rock, respectively. In the C_s-symmetry reactant, ion–molecule complex, $S_9 + S_{11}$ = CH_2 scissor; $S_9 - S_{11}$ = CH_2 wag; $S_{10} + S_{12}$ = CH_2 rock; $S_{10} - S_{12}$ = CH_2 twist. [d] Mathematical definition for linear bends: $\theta(i,j,k) = \sin^{-1}[\mathbf{e}_d \cdot (\mathbf{e}_{jk} \times \mathbf{e}_{ji})]$, where $\mathbf{e}_{jk}$ and $\mathbf{e}_{ji}$ are unit vectors directed from atom j to atoms k and i, respectively, and $\mathbf{e}_d$ is a fixed unit vector perpendicular to the plane of bending. For θ_a, $\mathbf{e}_d$ is directed into the plane of Figures 6 and 7, and for θ_b, $\mathbf{e}_d$ is directed from C_2 toward Cl_6.

methods.[122-124] These procedures were performed for the three important points along the S_N2 reaction coordinate using three basis sets: 3-21G, 6-31G, and 6-31+G(d,p). Integrated IR intensities were computed at the RHF level in the double-harmonic approximation.[125,126] Polarizability derivatives were also determined analytically with the RHF wave functions, thus allowing the prediction of Raman scattering activities using a well-known formula involving derivatives of the trace and anisotropy of the polarizability tensor with respect to the various normal coordinates.[127] Using the 6-311+G(d,p) basis set, frozen-core MP2 geometric structures were optimized via finite displacements of the symmetry coordinates since analytic derivatives were unavailable at this level of theory. These structures were converged to 10^{-4} Å or radians in the internal coordinates. The results of all geometry optimizations are presented in Tables III, IV, and V, and graphical representations of the structures are given in Figures 6 and 7.

(d) Scaled Quantum Mechanical Force Fields (SQM). Scaling of RHF force constants is desirable to eliminate potential sources

(122) Gaw, J. F.; Handy, N. C. *Annu. Rep. R. Soc. Chem., Sect. C* **1984**, 291.
(123) Schaefer, H. F., III; Yamaguchi, Y. *J. Mol. Struct.* **1986**, *135*, 369.
(124) Jørgensen, P.; Simons, J. *Geometrical Derivatives of Energy Surfaces and Molecular Properties*; Reidel: Dordrecht, 1986.
(125) Overend, J. In *Infrared Spectroscopy and Molecular Structure*; Davies, M., Ed.; Elsevier: Amsterdam, 1963; p 345.
(126) Zerbi, G. In *Vibrational Intensities in Infrared and Raman Spectroscopy*; Person, W. B., Zerbi, G., Eds.; Elsevier: Amsterdam, 1982.
(127) Frisch, M. J.; Yamaguchi, Y.; Gaw, J. F.; Schaefer, H. F., III; Binkley, J. S. *J. Chem. Phys.* **1986**, *84*, 531.

Table VIII. Spectral Data for the Vibrational Modes of Chloroacetonitrile ($ClCH_2CN$)

description of normal mode	assignment	ν (expt)[a]	ν (SQM)[b]	ω (RHF)[c]	infrared intensity[d]	Raman intensity[e]	total energy distribution[f]
CH_2 sym stretch	$\nu_1(a')$	2963	2957	3278	4.8	100.8 (77)	$S_3(100)$
C≡N stretch	$\nu_2(a')$	2256	2256	2616	3.7	86.0 (86)	$S_1(89) - S_2(11)$
CH_2 scissor	$\nu_3(a')$	1421	1427	1595	4.7	8.8 (9)	$S_7(68) + S_9(25) + S_6(6)$
CH_2 wag	$\nu_4(a')$	1270	1280	1438	40.8	6.9 (9)	$S_9(73) - S_7(26)$
C—C stretch	$\nu_5(a')$	930	929	1009	31.0	3.3 (5)	$S_2(77) + S_1(9) - S_5(6) + S_7(5)$
C—Cl stretch	$\nu_6(a')$	746	745	823	40.9	27.8 (75)	$S_5(66) - S_6(20) + S_{11}(11)$
C—C—Cl bend	$\nu_7(a')$	492	495	542	3.5	3.3 (16)	$S_{11}(36) - S_5(30) - S_6(26) - S_2(7)$
C—C≡N in-plane bend	$\nu_8(a')$	198	196	210	7.6	5.4 (34)	$S_{11}(52) + S_6(45)$
CH_2 antisym stretch	$\nu_9(a'')$	3010	3016	3344	0.7	57.1 (17)	$S_4(100)$
CH_2 twist	$\nu_{10}(a'')$	1184	1177	1324	1.0	6.1 (5)	$S_8(57) - S_{10}(41)$
CH_2 rock	$\nu_{11}(a'')$	907	898	1012	0.2	2.3 (2)	$S_{10}(58) + S_8(35) + S_{12}(7)$
C—C≡N out-of-plane bend	$\nu_{12}(a'')$	352	353	398	0.7	5.5 (11)	$S_{12}(91) - S_8(8)$

[a] Experimental vibrational frequencies in cm^{-1} taken from refs 131 and 135. [b] Scaled vibrational frequencies in cm^{-1} obtained from SQM analysis (see text). [c] Unscaled vibrational frequencies in cm^{-1} determined at the RHF 6-31+G(d,p) level of theory. [d] Theoretical infrared intensities in units of km mol^{-1} based on unscaled RHF 6-31+G(d,p) quadratic force fields. [e] Theoretical Raman scattering activities in units of $Å^4$ amu^{-1}, based on unscaled RHF 6-31+G(d,p) quadratic force fields; experimental values in parentheses (see text). [f] The percentage proportions, k, of the total energy (kinetic and potential) of the normal vibrations which can be ascribed to the individual internal coordinates S_i are indicated as $S_i(k)$ entries. The signs preceding these entries denote the relative phases of the internal coordinates in the normal-mode eigenvectors.

Table IX. Spectral Data for the Vibrational Modes of the C_s-Symmetry, [$ClCH_2CN \cdot Cl^-$] Complex

description of normal mode	assignment	ν (SQM)[a]	ω (RHF)[b]	infrared intensity[c]	Raman intensity[d]	total energy distribution[e]
CH_2 sym stretch	$\nu_1(a')$	2995	3322	13.4	103.5	$S_3(100)$
C≡N stretch	$\nu_2(a')$	2242	2600	17.3	94.8	$S_1(90) - S_2(10)$
CH_2 scissor	$\nu_3(a')$	1382	1548	48.5	12.5	$S_9(90) + S_7(5) + S_{11}(4)$
CH_2 wag	$\nu_4(a')$	1279	1437	42.0	9.3	$S_{11}(95) - S_9(5)$
C—C stretch	$\nu_5(a')$	917	993	35.0	2.5	$S_2(80) + S_1(9) - S_5(4)$
C—Cl stretch	$\nu_6(a')$	712	784	78.7	32.5	$S_5(61) - S_7(21) + S_{13}(14)$
C—C—Cl bend	$\nu_7(a')$	498	547	11.6	6.5	$S_5(36) - S_{13}(34) + S_7(24) + S_2(6)$
C—C≡N in-plane bend	$\nu_8(a')$	205	219	18.1	5.7	$S_{13}(49) + S_7(39) + S_6(9)$
C—Cl^- stretch	$\nu_9(a')$	104	105	21.5	0.1	$S_6(90) - S_7(7)$
C—Cl^- bend	$\nu_{10}(a')$	34	34	10.2	0.9	$S_8(100)$
CH_2 antisym stretch	$\nu_{11}(a'')$	3055	3387	14.6	44.3	$S_4(100)$
CH_2 twist	$\nu_{12}(a'')$	1176	1323	0.2	3.9	$S_{10}(57) - S_{12}(41)$
CH_2 rock	$\nu_{13}(a'')$	864	970	0.1	1.2	$S_{12}(56) + S_{10}(32) + S_{14}(9)$
C—C≡N out-of-plane bend	$\nu_{14}(a'')$	357	406	2.4	4.3	$S_{14}(91) - S_{10}(10)$
Cl^- out-of-plane torsion	$\nu_{15}(a'')$	44i	44i			$S_{15}(100)$

[a] Scaled vibrational frequencies in cm^{-1} obtained from SQM analysis (see text). [b] Unscaled vibrational frequencies in cm^{-1} determined at the RHF 6-31+G(d,p) level of theory. [c] Theoretical infrared intensities in units of km mol^{-1}. [d] Theoretical Raman scattering activities in units of $Å^4$ amu^{-1}. [e] See footnote *f* of Table VIII.

Table X. Spectral Data for the Vibrational Modes of the C_1-Symmetry, Hydrogen-Bonded [$ClCH_2CN \cdot Cl^-$] Complex

description of normal mode	assignment	ν (SQM)[a]	ω (RHF)[b]	infrared intensity[c]	Raman intensity[d]	total energy distribution[e]
CH_2 sym stretch	ν_1	2913	3230	207.7	235.6	$S_3(81) + S_4(19)$
C≡N stretch	ν_2	2240	2598	20.4	101.5	$S_1(90) - S_2(10)$
CH_2 scissor	ν_3	1409	1577	48.0	16.0	$S_9(81) + S_{11}(14) + S_7(5)$
CH_2 wag	ν_4	1297	1458	43.0	8.9	$S_{11}(84) - S_9(14)$
C—C stretch	ν_5	918	994	37.5	3.4	$S_2(79) + S_1(9) - S_5(4)$
C—Cl stretch	ν_6	717	790	75.7	28.7	$S_5(62) - S_7(21) + S_{14}(13)$
C—C—Cl bend	ν_7	367	416	4.3	5.2	$S_{13}(81) + S_{10}(9) - S_{14}(8)$
C—C≡N in-plane bend	ν_8	207	221	19.4	5.8	$S_{14}(42) + S_7(40) + S_6(10) + S_{13}(5)$
C—Cl^- stretch	ν_9	118	118	30.5	0.4	$S_6(89) - S_7(6)$
C—Cl^- bend	ν_{10}	66	66	18.4	0.8	$S_{15}(76) + S_8(23)$
CH_2 antisym stretch	ν_{11}	3014	3342	42.2	64.7	$S_4(81) - S_3(19)$
CH_2 twist	ν_{12}	1184	1332	2.0	3.9	$S_{10}(55) - S_{12}(41)$
CH_2 rock	ν_{13}	885	997	10.1	5.8	$S_{12}(56) + S_{10}(35) - S_{13}(7)$
C—C≡N out-of-plane bend	ν_{14}	499	549	10.1	5.1	$S_5(35) - S_{14}(32) + S_7(23) + S_2(7)$
Cl^- out-of-plane torsion	ν_{15}	44	44	9.8	1.3	$S_8(75) - S_{15}(24)$

[a] Scaled vibrational frequencies in cm^{-1} obtained from SQM analysis (see text). [b] Unscaled vibrational frequencies in cm^{-1} determined at the RHF 6-31+G(d,p) level of theory. [c] Theoretical infrared intensities in units of km mol^{-1}. [d] Theoretical Raman scattering activities in units of $Å^4$ amu^{-1}. [e] See footnote *f* of Table VIII.

of error in the RRKM computations due to uncertainties in vibrational frequencies. A scheme for combining empirical and ab initio data which has been widely adopted and extensively developed is the scaled quantum mechanical (SQM) force field method of Pulay and co-workers.[128-133] The implementation of the SQM procedure used here is described in a recent paper by Allen and co-workers.[134]

(128) Fogarasi, G.; Pulay, P. In *Vibrational Spectra and Structure*; Durig, J. R., Ed.; Elsevier: Amsterdam, 1985; p 125.

(129) Pulay, P.; Fogarasi, G.; Boggs, J. E. *J. Chem. Phys.* **1981**, *74*, 3999.

(130) Pulay, P.; Fogarasi, G.; Pongor, G.; Boggs, J. E.; Vargha, A. *J. Am. Chem. Soc.* **1983**, *105*, 7037.

(131) Banhegyi, G.; Forgarasi, G.; Pulay, P. *J. Mol. Struct.* **1982**, *89*, 1.

(132) Pongor, G.; Pulay, P.; Fogarasi, G.; Boggs, J. E. *J. Am. Chem. Soc.* **1984**, *106*, 2765.

Table XI. Spectral Data for the Vibrational Modes of the C_{2v}-Symmetry, $[Cl_2CH_2CN^-]^‡$ S_N2 Transition State

description of normal mode	assignment	ν (SQM)[a]	ω (RHF)[b]	total energy distribution[c]
CH_2 sym stretch	$\nu_1(a_1)$	3138	3479	$S_3(100)$
C≡N stretch	$\nu_2(a_1)$	2257	2614	$S_1(88) - S_2(12)$
CH_2 scissor	$\nu_3(a_1)$	1385	1555	$S_9(97)$
C—C stretch	$\nu_4(a_1)$	968	1049	$S_2(82) - S_1(12)$
CCl_2 sym stretch	$\nu_5(a_1)$	196	220	$S_5(100)$
C—C—Cl sym bend	$\nu_6(a_1)$	161	162	$S_7(97)$
CH_2 twist	$\nu_7(a_2)$	901	1013	$S_{12}(99)$
CH_2 antisym stretch	$\nu_8(b_1)$	3270	3624	$S_4(100)$
CH_2 rock	$\nu_9(b_1)$	1002	1123	$S_{11}(94) - S_6(4)$
C—C≡N out-of-plane bend	$\nu_{10}(b_1)$	375	425	$S_{14}(89) + S_{10}(9)$
Cl–C–C–Cl torsion	$\nu_{11}(b_1)$	214	214	$S_{15}(96)$
CH_2 wag	$\nu_{12}(b_2)$	999	1122	$S_{10}(90) - S_{14}(8)$
C—C≡N in-plane bend	$\nu_{13}(b_2)$	476	524	$S_{13}(70) + S_8(35) + S_6(-4)$
CCl_2 antisym bend	$\nu_{14}(b_2)$	165	172	$S_8(72) + S_{13}(31)$
CCl_2 antisym stretch	$\nu_{15}(b_2)$	508i	509i	$S_6(103) - S_8(-7) - S_{11}(4)$

[a] Scaled vibrational frequencies in cm^{-1} obtained from SQM analysis (see text). [b] Unscaled vibrational frequencies in cm^{-1} determined at the RHF 6-31+G(d,p) level of theory. [c] See footnote *f* of Table VIII.

For the study of eq 2, seven distinct scale factors were employed, as detailed in Table VI. All results were based on 6-31+G(d,p) RHF quadratic force fields determined at the corresponding optimum geometries. The definitions of the symmetry coordinates (S_i) for the relevant structures involved in the analyses are given in Table VII. The values for the unique scale factors were found by performing a least-squares fit to the experimental fundamental frequencies of $ClCH_2CN$.[135] In the SQM analyses of the various stationary points along the S_N2 reaction path of the $[Cl_2CH_2CN]^-$ system, the scale factors obtained for $ClCH_2CN$ were applied as fixed parameters. Vibrational modes formed during the reaction were left unscaled. Spectral and normal coordinate analysis data for the four stationary points of interest are given in Tables VIII, IX, X, and XI. The characterization of the normal modes in these tables is achieved by means of the total energy distribution (TED) advocated by Pulay and Török.[136]

B. Ab Initio Theoretical Results. (a) Geometric Structures. For most organic systems, Hartree–Fock theory underestimates bond distances by 0.01–0.03 Å, depending on the order of the bond.[137] Such disparities are usually mitigated at the MP2 level, but with basis sets of only moderate size, overestimations of bond distances by 0.01–0.02 Å may result.[137] These expectations are borne out in the data for the structure of chloroacetonitrile in Table III. In the RHF results, the addition of the first set of polarization functions to the basis set is seen to be critical in reproducing the C_3–Cl_6 distance (nota bene the 6-31+G and 6-31+G(d,p) values differ by 0.08 Å), but subsequent augmentations of the one-particle basis yield only modest changes. The general agreement between the experimental microwave structures and the best theoretical results in Table III is very good, and the empirical C_3–H_4 and C_3–Cl_6 distances of Wada et al.[139] appear to be preferred. Chemically significant observations pertaining to the geometric structure of chloroacetonitrile are that the C_2–N_1 and C_3–Cl_6 distances are essentially the same as the r(C≡N) = 1.153 Å[140] value in HCN and the r(C–Cl) = 1.781 Å[137] distance in CH_3Cl, respectively, whereas the C_2–C_3 length is substantially shorter than the prototypical 1.54-Å carbon–carbon single-bond distance.

The theoretical data for the geometric structure of the $[ClCH_2CN{\cdot}Cl^-]$ complex are presented in Table IV. The changes in the structural parameters of the chloroacetonitrile moiety upon complexation are generally minuscule, the 0.02-Å elongation of the C_3–Cl_6 distance being the most significant. Accurate predictions of both the C_3–Cl_6 and C_3–Cl_7 distances are seen to require basis sets of at least 6-31+G(d,p) quality. At the 6-311+G(d,p) RHF level, the C_3–Cl_7 distance in the C_s-symmetry complex is 3.344 Å, but the analogous MP2 distance is smaller by a full 0.16 Å. Further expansion of the basis set with simultaneous incorporation of electron correlation decreases $r(C_3$–$Cl_7)$ even more. By computing four TZ3P+R+(2f,d) MP2 energy points for C_3–Cl_7 distances in the range 2.8–3.2 Å while maintaining all other geometric coordinates at the 6-31+G(d,p) MP2 values, a final prediction of $r(C_3$–$Cl_7)$ = 3.118 Å is obtained for the C_s-symmetry complex. In addition to $r(C_3$–$C_7)$, the angle $\alpha(Cl_7$–C_3–$C_2)$ is sensitive to level of theory. Note that the smaller values are strongly correlated with associated predictions of short C_3–Cl_7 distances. In essence the C_3–Cl_7 separation determines the degree to which the Cl^- ion is deflected from the asymptotic angle of approach, $\alpha(Cl_7$–C_3–$C_2)$ = 156.8°, given by the direction of the dipole moment of the neutral. The exact Cl_7–C_3–C_2 angle is anticipated to be slightly smaller than the 109.60° value at the 6-311+G(d,p) MP2 level, because the corresponding value of $r(C_3$–$Cl_7)$ is reduced at higher levels of theory.

As revealed in Table IX, the C_s-symmetry, backside S_N2 complex of Figure 6 is not a local minimum at the 6-31+G(d,p) RHF level of theory in that one normal mode of a″ symmetry has an imaginary frequency of 44i cm^{-1}. The eigenvector for this mode is almost purely composed of Cl_7 out-of-plane bending motion, leading to a hydrogen-bonded complex in C_1 symmetry (Figure 6). At the 6-31+G(d,p) RHF level the C_1 minimum lies only 0.17 kcal mol^{-1} lower in energy than the C_s structure, but the differences resulting in some of the geometric parameters are substantial. In the C_s complex the Cl_7–H_4 distance is 2.846 Å and the C_3–H_4 length is 1.076 Å. In going to the C_1-symmetry complex, $r(Cl_7$–$H_4)$ contracts to 2.439 Å and $r(C_3$–$H_4)$ concomitantly elongates to 1.083 Å, in accord with the expected weakening of the covalent, C_3–H_4 bond as the electrostatic, Cl_7–H_4 hydrogen bond is strengthened. In free chloroacetonitrile, the nitrile group is slightly trans-bent relative to the chlorine substituent, i.e., $\tau(Cl_6$–C_3–C_2–$N_1)$ = 180°. At all levels of theory except 6-31+G RHF, the trans arrangement is maintained in the C_s-symmetry complex. The final position of the Cl^- ion in the C_1-symmetry complex is easily envisioned by noting the 34.6° deviation of the $\tau(Cl_7$–C_3–C_2–$Cl_6)$ dihedral angle from its original value of 180°.

Theoretical geometric structures for the S_N2 transition state of $[Cl_2CH_2CN^-]$ are given in Table V, where good convergence of the RHF predictions with respect to basis set enlargement is seen for most parameters. The most prominent internal coor-

(133) Sellers, H.; Pulay, P.; Boggs, J. E. *J. Am. Chem. Soc.* **1985**, *107*, 6487.
(134) Allen, W. D.; Császár, A. G.; Horner, D. A. *J. Am. Chem. Soc.* **1992**, *114*, 6834.
(135) Durig, J. R.; Wertz, D. W. *Spectrochim. Acta A* **1968**, *24*, 21.
(136) Pulay, P.; Török, F. *Acta Chim. Acad. Sci.* **1966**, *47*, 273.
(137) Hehre, W. J.; Radom, L.; Schleyer, P. v. R.; Pople, J. A. In *Ab Initio Molecular Orbital Theory*; Wiley-Interscience: New York, 1986.
(138) Lee, T. J.; Allen, W. D.; Schaefer, H. F., III *J. Chem. Phys.* **1987**, *87*, 7062 and references therein. Allen, W. D.; Yamagnchi, Y.; Császár, A. G.; Clabo, D. A., Jr.; Remington, R. B.; Schaefer, H. F., III *Chem. Phys.* **1990**, *145*, 427 and references therein.
(139) Wada, K.; Kikachi, Y.; Matsumura, C.; Hirota, E.; Morino, Y. *Bull. Chem. Soc. Jpn.* **1961**, *34*, 337.
(140) Winnewisser, G.; Maki, A. G.; Johnson, D. R. *J. Mol. Spectrosc.* **1971**, *39*, 149.

Table XII. Complexation Energy[a] (kcal mol^{-1}) for $ClCH_2CN + Cl^- \rightarrow [ClCH_2CN{\cdot}Cl]^-$

level of theory	RHF	MP2	MP3	MP4
3-21G	19.20 (19.80)	18.58	18.61	18.68
6-31G	18.41 (18.80)	17.97	18.02	18.20
6-31+G	16.38 (16.94)	16.19	16.28	16.57
6-31+G(d,p)	15.29 (15.71)	17.23 (17.08)	17.09 (17.02)	17.23 (17.11)
6-311+G(d,p)	15.45 (15.86)	17.92	17.80	17.94
6-311+G(2d,2p)	15.68 (15.99)	18.56 (18.19)		
TZ2P+R+f	15.40	18.50		
TZ3P+R+(2f,d)	15.48	18.27		

Final predictions: D_e = 18.4 kcal mol^{-1}, D_0 = 18.2 kcal mol^{-1}, ΔE_{well} = 18.4 kcal mol^{-1}.

[a] The principal entries in the table were determined at the 6-311+G(d,p) MP2 geometries, whereas the values in parentheses correspond to optimized RHF structures for the basis set given.

dinates, the C_3–$Cl_{6,7}$ distances, are somewhat less sensitive to level of theory than in the case of the ion–molecule complex. As the basis set is augmented from 6-31+G to 6-31+G(d,p), $r(C_3$–$Cl_{6,7})$ is shortened by 0.048 Å rather than elongated by 0.046 Å as found before for $r(C_3$–$Cl_7)$. The MP2 procedure with the 6-311+G(d,p) basis contracts the C_3–$Cl_{6,7}$ distances further, but only by 0.068 Å, as compared to 0.163 Å in the ion–molecule complex. The final prediction for $r(C_3$–$Cl_{6,7})$ is 2.274 Å,[141] this result being obtained as before from a one-parameter re-optimization at the TZ3P+R+(2f,d) MP2 level while fixing the remaining coordinates at their 6-311+G(d,p) MP2 values. Accordingly, the two equivalent C–Cl distances are found to be quite short, and the S_N2 transition state is tight in character.

Other noteworthy results in Table V pertain to the bonding about the central carbon atom. The C_3–C_2 distance is only approximately 0.05 Å longer than the carbon–carbon distance in benzene. Moreover, in Tables III–V the $\alpha(H_{4,5}$–C_3–$C_2)$ angle varies monotonically from ca. 109.5° in chloroacetonitrile itself to near 120° in the S_N2 transition state. Both of these observations support the view that the central carbon in the transition-state structure is indeed sp^2 hybridized with a substantial degree of π bonding occurring with the nitrile framework. Such a bonding description is also qualitatively consistent with the unusually short C–H distances reported in Table V. In fact, the 6-31+G(d,p) RHF carbon–hydrogen distance of 1.0602 Å is even 0.016 Å shorter than the 6-31G(d,p) RHF value in ethylene and only 0.003 Å longer than the analogous C–H distance in acetylene.[138] The conclusion that the carbon–hydrogen distances in the S_N2 transition state are intermediate between prototypical C(sp^2)–H and C(sp)–H bond lengths is also apparent from comparisons of analogous MP2 structures. Further analysis of the bonding in the S_N2 transition state is reserved for the discussion of electronic structure given below.

(b) Vibrational Frequencies. All 12 fundamental vibrations of chloroacetonitrile have been characterized previously in a normal coordinate analysis by Crowder[142] of the experimental infrared and Raman spectra of Durig and Wertz.[135] As shown in Table VIII, the SQM fit to the empirical fundamental frequencies is excellent; moreover, the total energy distributions (TEDs) are in remarkable agreement with the potential energy distributions (PEDs) reported in Tables 4 and 5 of ref 142. Nevertheless, the interaction constants in the complete quadratic force field from the SQM analysis are much more complete and well determined than those previously obtained. The SQM force constants are available as supplementary material to this paper. Finally, Durig and Wertz[135] report relative Raman intensities for liquid-phase chloroacetonitrile, which can be compared to the ab initio gas-phase values by assuming in both cases an absolute scattering activity of 86.0 Å amu^{-1} for the intense ν_2 band. The experimental and theoretical values shown in Table VIII are indeed in qualitative accord, notwithstanding condensed-phase effects on the former values and basis-set deficiencies inherent in the latter predictions.

Spectral predictions for the C_s- and C_1-symmetry $[ClCH_2C$-$N{\cdot}Cl]^-$ complexes appear in Tables IX and X. The 44i cm^{-1} frequency for $\nu_{15}(a'')$ of the C_s complex, which indicates the existence of a C_1-symmetry, hydrogen-bonded conformation, was highlighted above. In fact, with the 3-21G and 6-31G RHF wave functions, $\nu_{15}(a'')$ is evaluated as 74.5 and 43.5 cm^{-1}, respectively; thus, the C_s-symmetry, S_N2 backside complex is actually a local minimum at lower levels of theory. However, neither the 3-21G nor the 6-31G basis contains sets of diffuse s and p orbitals or d polarization functions on the heavy atoms, and the corresponding predictions of a C_s minimum are thereby vitiated.

At the 6-31+G(d,p) RHF level, the C≡N, C—C, and C—Cl distances of chloroacetonitrile are all slightly elongated upon complexation to the hydrogen-bonded C_1-symmetry structure. As expected, these geometry shifts are accompanied by slight downward shifts of 10–30 cm^{-1} in the corresponding stretching frequencies (cf. Tables VIII and X). The hydrogen bonding of Cl^- to chloroacetonitrile affects none of the CH_2 deformation frequencies by more than 20 cm^{-1}, but the C—C≡N out-of-plane bend becomes strongly coupled with other modes and is raised in frequency by almost 150 cm^{-1}. The newly-quantized vibrational modes formed upon complexation have normal frequencies of 118, 66, and 44 cm^{-1}, these correlating to weaker modes at 104, 34, and 44i cm^{-1} in the C_s-symmetry conformation. The effect of Cl^- binding on the infrared and Raman intensities of $ClCH_2CN$ is pronounced in many cases with a general trend toward enhancement of these quantities in the ion–molecule complex.

The vibrational frequencies in Table XI for the C_{2v}-symmetry stationary point confirm its existence as a true transition state. In particular, the antisymmetric C–Cl stretch, $\nu_{15}(b_2)$, occurs at 508i cm^{-1}. The 6-31G RHF structure in Table IV also has a Hessian index of 1, and in this case ν_{15} is predicted to be 398i cm^{-1}. A peculiar feature of the S_N2 transition state is the unusual magnitude of the C–H stretching frequencies (3138 and 3270 cm^{-1}), in accord with the bond-length observations made above. For comparison, the C–H stretching fundamentals of ethylene lie in the range 2989–3105 cm^{-1},[138] whereas those of acetylene occur at 3288 and 3373 cm^{-1}.[138] Evidence of enhanced π bonding along the C–C–N framework in the transition state is seen in the upward shifts of the C—C≡N bends in the neutral from 198 and 352 cm^{-1} to 375 and 476 cm^{-1}, respectively. The accompanying shift in the C–C stretch is from 930 to 968 cm^{-1}. Finally, three of the CH_2 deformation frequencies in the transition state are shifted substantially downward relative to the neutral while the CH_2 rocking frequency moves 100 cm^{-1} higher.

(c) Energetics. Theoretical predictions for the complexation energy (D_e) of Cl^- with chloroacetonitrile are given in Table XII. In general, the sensitivity of D_e to level of theory is quite modest. Diffuse basis functions are expected to be more important in describing the Cl^- ion than the ion–molecule complex because there is no means for dispersing the excess charge in the bare ion without the aid of Rydberg functions. The effect is to decrease D_e by ca. 2 kcal mol^{-1} when diffuse atomic orbitals are added, as seen by comparing the 6-31G and 6-31+G RHF results in Table XII. At

(141) Wolfe and co-workers (ref 157) have shown that the postulate of conservation of bond order (refs 158–160) is useful in the estimation of geometries for transition states of S_N2 cross reactions. To apply the postulate, the proportionality constants, a_x, in the Pauling bond-order relationship, (ref 161) R-$R_e = a_x \ln(n_x)$, must be determined for a series of identity exchange reactions. At the transition state of eq 2, the C–Cl bond order, n_x, is 0.5, and R = 2.27 Å. In the neutral, R_e = 1.78 Å, whence a_x = –0.707 Å^{-1}. This value should be useful in studying various S_N2 cross reactions involving chloroacetonitrile.

(142) Crowder, G. A. *Mol. Phys.* **1972**, *23*, 707.

Table XIII. S_N2 Barrier Height[a] (E_b, kcal mol^{-1}) for $ClCH_2CN + Cl^-$

level of theory	RHF	MP2	MP3	MP4
3-21G	−13.02 (−12.51)	−16.57	−14.73	−17.81
6-31G	−7.19 (−8.30)	−11.66	−9.70	−13.26
6-31+G	−2.77 (−4.01)	−7.45	−5.40	−9.43
6-31+G(d,p)	+7.00 (+5.67)	−0.26 (+0.69)	+2.63 (+3.01)	−1.80 (−1.48)
6-311+G(d,p)	+7.14 (+5.97)	−0.68	+2.49	−2.25
6-311+G(2d,2p)	+5.80 (+4.78)	−5.68 (−4.62)		
TZ2P+R+f	+6.76	−4.89		
TZ3P+R+2f,d	+6.88	−4.55		

Final predictions: E_b = −6.6 kcal mol^{-1}, ΔE_{diff} = −6.9 kcal mol^{-1}.

[a] The principal entries in the table were determined at the 6-311+G(d,p) MP2 geometries, whereas the values in parentheses correspond to optimized RHF structures for the basis set given.

the RHF level, polarization functions also lead to the reduction of D_e, but only by ca. 1 kcal mol^{-1} (cf. the 6-31+G and 6-311+G(d,p) RHF values). If the one-particle basis set is polarized, electron correlation is seen to increase D_e by ca. 2 kcal mol^{-1} as a consequence of dispersion effects in the interaction of the ion and neutral fragments. Finally, the sensitivity of the interfragment separation to level of theory gives rise to a geometric effect of the order of a few tenths of a kcal mol^{-1}.

The TZ2P+R+f and TZ3P+R+(2f,d) results indicate that the best predictions for D_e are essentially converged at both the RHF and MP2 levels of theory. The MP∞ values for D_e determined at the 6-311+G(d,p) MP2 geometry with the 3-21G, 6-31G, 6-31+G, 6-31+G(d,p), and 6-311+G(d,p) basis sets are 18.78, 18.33, 16.68, 17.15, and 17.98 kcal mol^{-1}, respectively, essentially the same as the corresponding MP2, MP3, and MP4 results. Thus, it is concluded that the prediction of D_e = 18.27 kcal mol^{-1} at the TZ3P+R+(2f,d) MP2 level would not be altered significantly by further improvements in the correlation treatment.

All of the D_e values in Table XII actually correspond to the well depth for the C_s-symmetry, S_N2 backside complex. The hydrogen-bonded complex in C_1 symmetry lies only 0.17 kcal mol^{-1} lower in energy at the 6-31+G(d,p) RHF level. The potential energy surface thus appears to be flat with respect to hydrogen-bond reorientation, a feature which is not expected to change with electron correlation. In brief, a final prediction of 18.4 kcal mol^{-1} accrues for the true D_e of the hydrogen-bonded complex. The SQM vibrational frequencies in Tables VIII and IX indicate a ZPVE correction to the well depth of only 0.21 kcal mol^{-1}, whence D_0 = 18.2 kcal mol^{-1}. The quantity ΔE_{well} in Figure 3 differs from D_0 only by the vibrational energy corresponding to quantization of the reaction-coordinate (R) motion, which is appropriately ascribed to ν_9 in Table IX. Thus, the final ΔE_{well} prediction is 18.36 kcal mol^{-1}.

Predictions for the vibrationless S_N2 barrier height (E_b) relative to reactants at various levels of theory are tabulated in Table XIII. In contrast to D_e, the barrier height is very sensitive to level of theory. Once again, in the RHF results diffuse and polarization functions selectively lower the reactants relative to the $[Cl_2CH_2CN]^-$ system, but in this case much more dramatically. Note that E_b varies from −13.0 to +7.0 kcal mol^{-1} in going from the 3-21G to the 6-31+G(d,p) RHF level of theory. Further enhancements of the basis set from 6-31+G(d,p) to TZ3P+R+(2f,d) do not change the RHF results significantly, but the MP2 predictions vary about 5 kcal mol^{-1} over this range. Nevertheless, the TZ3P+R+(2f,d) MP2 value of E_b = −4.55 kcal mol^{-1} appears to lie very near the basis set limit. While the correlation effect on E_b is ca. 11 kcal mol^{-1}, most of this shift is recovered at the MP2 level. The MP∞ − MP2 differences in E_b are −1.73, −2.18, −2.63, −2.85, and −1.86 kcal mol^{-1} with the 3-21G, 6-31G, 6-31+G, 6-31+G(d,p), and 6-311+G(d,p) basis sets, respectively. Because these differences vary only slightly, it is appropriate to propose a final value of E_b = −6.6 kcal mol^{-1} as obtained by appending an additional correlation correction of −2 kcal mol^{-1} to the TZ3P+R+(2f,d) MP2 value. The ΔE_{diff} quantity in Figure 3 differs from E_b by a zero-point vibrational correction for the modes orthogonal to the reaction path. The SQM data in Tables VIII and XI indicate this correction to be −0.32 kcal mol^{-1}, and thus ΔE_{diff} = −6.9 kcal mol^{-1}.

C. Electronic Structure of the S_N2 Transition State. The presence of the nitrile group in $ClCH_2CN$ has a dramatic effect on the stability of the S_N2 transition state for chloride exchange vis-à-vis the analogous critical configuration of the prototypical CH_3Cl/Cl^- reaction. The ab initio data presented in Tables V, XI, and XIII provide for the quantitative characterization of the $[Cl_2CH_2CN]^{\ddagger-}$ transition state and give a basis from which qualitative models of electronic structure can be constructed. Indeed, the quality of the ab initio results reported here for the $ClCH_2CN/Cl^-$ system necessitates the determination of improved theoretical data for CH_3Cl/Cl^- before proper comparisons can be made.

To determine improved values for ΔE_{well} and ΔE_{diff} of the CH_3Cl/Cl^- system (cf. Figure 3), 6-31+G(d,p) MP2–MP4 and TZ3P+R+(2f,d) RHF and MP2 energy points were obtained at the 6-31G(d,p) MP2 geometric structures of Tucker and Truhlar.[50] The resulting TZ3P+R+(2f,d) RHF predictions are ΔE_{well} = −8.15 and ΔE_{diff} = +7.59 kcal mol^{-1},[143] both of which must closely approach the Hartree–Fock limit. For comparison, the best RHF results reported previously (−9.0 and +5.7 kcal mol^{-1}, respectively) are those obtained by Vetter and Zülicke with a basis set of DZP+R quality.[51] The TZ3P+R+(2f,d) MP2 predictions for the CH_3Cl/Cl^- system are ΔE_{well} = −10.51 and ΔE_{diff} = +3.54 kcal mol^{-1}. The latter result is significantly lower than other previous estimates.[51,52] Finally, the 6-31+G(d,p) MP4–MP2 *corrections* for ΔE_{well} and ΔE_{diff} are −0.1 and −1.7 kcal mol^{-1}, respectively, essentially the same as the MP∞ − MP2 differences. Appending these corrections to the TZ3P+R+(2f,d) MP2 results gives the final predictions ΔE_{well} = −10.6 and ΔE_{diff} = +1.8 kcal mol^{-1}, which are analogous to the final values proposed in Tables XII and XIII for $ClCH_2CN/Cl^-$.

Energetic predictions for the CH_3Cl/Cl^- reaction profile are depicted in Figure 8 along with the corresponding $ClCH_2CN/Cl^-$ curves. Note that the RHF values of ΔE_{diff} for the two systems are nearly identical, near 7 kcal mol^{-1} in both cases. Therefore, *the dramatic stabilization of the S_N2 transition state of the $ClCH_2CN/Cl^-$ system relative to reactants arises solely from electron correlation effects.* Whereas the difference in energy between the ion–molecule complex and the S_N2 transition state, ΔE^*, is 22.1 kcal mol^{-1} at the RHF level, it is only 11.4 kcal mol^{-1} upon inclusion of electron correlation. The correlated value of ΔE^* for CH_3Cl is remarkably similar, viz. 12.4 kcal mol^{-1}. Two conclusions then become apparent. *First, no bonding model based on molecular orbital concepts alone can provide a valid explanation of the unusually low S_N2 barrier height relative to separated reactants for eq 2 compared to eq 1, because in the Hartree–Fock limit the ΔE_{diff} values are almost indistinguishable. Second, because the correlated values of ΔE^* in the two cases are nearly the same, the stabilization of the S_N2 transition state for the $ClCH_2CN/Cl^-$ system is ultimately a consequence of the increased chloride-ion binding energy which occurs upon nitrile substitution.* As discussed in Section II, this enhanced binding is electrostatic in origin.

(143) The zero-point vibrational corrections to D_e and E_b (see Section IV) used to evaluate ΔE_{well} and ΔE_{diff} were +0.1 and −0.6 kcal mol^{-1}, respectively, as calculated from the 6-31(d) RHF vibrational frequencies of Tucker and Truhlar (ref 50).

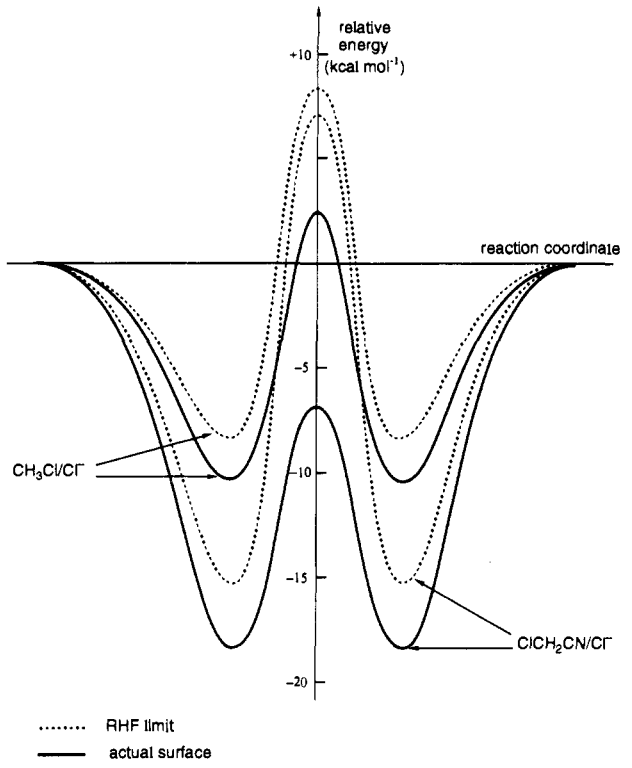

Figure 8. Potential energy profiles for the S_N2 identity exchange reaction of $ClCH_2CN$ and CH_3Cl with Cl^-.

Scheme III

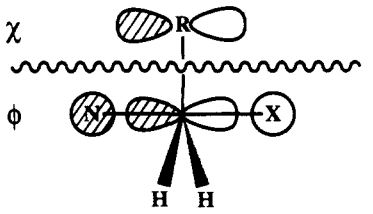

The importance of electron correlation in the S_N2 barrier for the $ClCH_2CN/Cl^-$ system is indicated by the relative tightness of the transition state, but not in a conspicuous way. To wit, the C–Cl distances determined here for $ClCH_2CN/Cl^-$ are about 0.02 Å shorter than analogous values reported by Tucker and Truhlar[50] for the CH_3Cl/Cl^- transition state. However, the symmetric C–Cl stretching frequencies (near 200 cm^{-1}) are not substantially different, and in both cases unusually short C–H bonds are found.

Frontier molecular orbital (FMO) models have been used by several investigators to rationalize α-substituent effects in S_N2 reactions.[144-147] At the S_N2 transition state a high-lying, occupied molecular orbital, ϕ, of π symmetry extends over the bonding region involving the reaction center, nucleophile (N), and leaving group (X), as shown in Scheme III. If the α substituent (R) on the central carbon has a low-lying, unoccupied π-type orbital, χ, which is properly oriented for strong overlap with ϕ, then a relative stabilization of the transition state occurs. In contrast, if χ is occupied by lone-pair electrons in the substituent, then a relative destabilization of the transition state arises. Such FMO considerations have been used to explain the general S_N2 reactivity trends $CH_3OCH_2Cl > CH_3Cl > CH_2Cl_2$.[144] In the CH_3OCH_2Cl case, the CH_3O substituent stabilizes the transition state vis-ã-vis CH_3Cl by σ induction, while averting destabilization due to π donation because the χ orbital is rotated 90° relative to ϕ.

Scheme IV

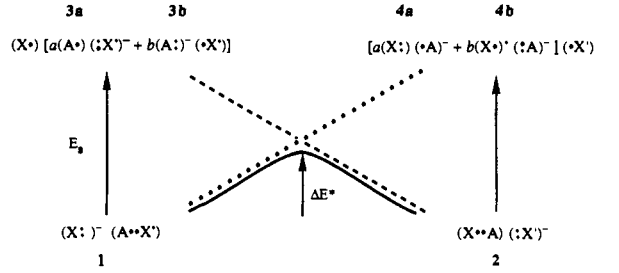

However, in the CH_2Cl_2 case repulsion from a lone pair of electrons in the Cl substituent cannot be avoided, and the transition state is destabilized in a relative sense.

In the case of chloroacetonitrile, a π^* orbital in the CN group functions as the orbital χ in Scheme III. Thus the FMO model predicts that the C–C distance in the S_N2 transition state is somewhat shorter than in the ion–molecule complex while the C–N distance is slightly longer. As seen in Tables IV and V, the expected contraction of the C–C distance by ca. 0.02 Å is indeed observed, but elongation of the C–N bond only occurs after electron correlation is included. The simple FMO model also predicts a delocalization of excess charge into the π system of the nitrile framework, but previous computational evidence for carbonyl substituents[145] suggests that this charge transfer would be largely cancelled by polarization of the C–C σ bond in the opposite direction. In fact, the Mulliken population analyses performed here with the 6-311+G(d,p) basis set reveal that the net charge on the CN moiety is –0.17 in the neutral and –0.38 in the ion–molecule complex, but only –0.02 in the S_N2 transition state. Hence charge appears to actually flow out of the nitrile group as the S_N2 critical configuration is reached. In brief, the simple FMO model is at variance with several structural features of the S_N2 transition state. The inadequacy of the model is not surprising given that the molecular-orbital approximation itself, i.e., Hartree–Fock theory, predicts ΔE^* for the $ClCH_2CN/Cl^-$ system to be 7 kcal mol^{-1} *greater* than that for the CH_3Cl/Cl^- prototype.

A qualitative bonding description which is more successful in rationalizing the different reaction profiles of eqs 1 and 2 is the valence bond configuration mixing (VBCM) model of Shaik and co-workers.[148-153] The concepts of VBCM have been fully developed over the past 10 years and have been applied to a variety of reactions in solution as well as in the gas phase. The rudiments of the model, as applied to S_N2 identity exchange reactions, are illustrated in Scheme IV, where X represents the nucleophile and AX′ the substrate (X and X′ are chemically equivalent). The reference valence bond configurations for the reactants and products are denoted as **1** and **2**, respectively. Charge transfer from the nucleophile to the substrate gives rise to electronic structure **3**, which is a mixture of valence bond forms **3a** and **3b**. An equivalent structure **4** exists for the products. The crux is that the S_N2 barrier results from an avoided crossing of the electronic curves for **3** → **2** and **1** → **4**. The donor–acceptor gap, E_g, between **1** and **3** is merely the difference between the ionization potential of the nucleophile and the vertical electron affinity of the substrate. In the analysis by Shaik,[148] the height of the barrier, ΔE^*, is modeled by the expression $\Delta E^* = fE_g$, where f is simply a fraction which depends on the steepness of descent of the **3** → **2** curve at the transition state. If f remains approximately constant for a series of reactions, then clearly the corresponding activation barriers ΔE^* are directly proportional to the donor–acceptor gaps. However, variations in f are important aspects of the model.

(144) Kost, D.; Aviram, K. *Tetrahedron Lett.* **1982**, *23*, 4157.
(145) Pross, A.; Aviram, K.; Klix, R. C.; Kost, D.; Bach, R. D. *Nouv. J. Chim.* **1984**, *8*, 711.
(146) Shaik, S. S.; Duzy, E.; Bartuv, A. *J. Phys. Chem.* **1990**, *94*, 6574.
(147) Wolfe, S.; Mitchell, D. J.; Schlegel, H. B.; Minot, C.; Eisenstein, O. *Tetrahedron Lett.* **1982**, *23*, 615.
(148) Shaik, S. S.; Schlegel, H. B.; Wolfe, S. *Theoretical Aspects of Physical Organic Chemistry: The S_N2 Mechanism*; Wiley-Interscience: New York, 1992.
(149) Shaik, S. S. *J. Am. Chem. Soc.* **1983**, *105*, 4358.
(150) Shaik, S. S. *J. Am. Chem. Soc.* **1981**, *103*, 3692. Pross, A.; Shaik, S. S. *J. Am. Chem. Soc.* **1981**, *103*, 3702.
(151) Shaik, S. S.; Pross, A. *J. Am. Chem. Soc.* **1982**, *104*, 2708.
(152) Shaik, S. *Nou. J. Chim.* **1982**, *6*, 159.
(153) Shaik, S. S. *J. Am. Chem. Soc.* **1984**, *106*, 1227.

According to Shaik and co-workers, as the ability of the substrate to delocalize charge away from the reaction center increases, structure **3b** becomes more important relative to **3a**, and consequently the **3** → **2** curve becomes flat in the initial stages of the reaction. Under these circumstances f is relatively large. In contrast, if there is an initial localization of charge in the substrate, **3a** predominates over **3b**, and a relatively small value of f results. In summary, in the VBCM model constructed by Shaik et al., the magnitude of the activation barrier for an S_N2 reaction depends on the interplay between the donor–acceptor energy gap and delocalization of the excess charge transferred to the reaction center.

In the ion–molecule complexes of [$ClCH_2CN{\cdot}Cl^-$] and [$CH_3Cl{\cdot}Cl^-$], nearly all of the stabilization relative to separated reactants arises from electrostatics alone and can be accounted for by considering a point charge in the full multipole field of the neutral (see Section II). In brief, formation of the ion–molecule complexes does not involve substantial changes in electronic structure. This conclusion is likely to be valid for most substrates, at least those reacting with Cl^-. Therefore, in applying the VBCM model, the reactants and products in Scheme IV are those species that exist immediately before and after the substitution step, these being the two chemically equivalent ion–molecule complexes. The activation energy referred to in the model is thus the energy difference between the ion–molecule complex and the S_N2 transition state, which is consistently denoted as ΔE^* here. Otherwise, the effects of long-range electrostatic interactions spoil the analysis, and the qualitative reaction profiles in Figure 8 and Scheme IV do not match.

According to Shaik,[149] the two effects which govern the value of ΔE^* are in competition for many systems and often very nearly cancel one another. In substrates with π systems α to the reaction center, enhanced electron affinities arise because low-lying, unoccupied π^* orbitals are present, but at the same time resonance delocalization of excess charge transferred to the reaction center is facilitated. In comparing eqs 1 and 2 according to the VBCM model, Shaik[149] has attempted to quantify the competition between gap and slope, or delocalization, factors by calculating relative barrier heights within the formalism. For the CH_3Cl substrate, $E_g \approx 113$ kcal mol^{-1} and $f \approx 0.25$, whereas for $ClCH_2CN$ these values are about 88 kcal mol^{-1} and 0.32, respectively. The E_g and f factors balance one another to the extent that the ΔE^* values differ by only 0.2 kcal mol^{-1}, CH_3Cl having the lower barrier. These predictions cannot be regarded as quantitative, although there is good agreement with the final ab initio value for the ΔE^* difference between the two systems, i.e., 1 kcal mol^{-1}, but with $ClCH_2CN$ having the lower barrier. Whether such agreement between a qualitative bonding model and rigorous ab initio quantum mechanical computations is fortuitous or fundamental is by no means clear. Shi and Boyd[154] have criticized the form of the VBCM wave function, but their objections pertain primarily to S_N2 cross reactions, not identity exchange processes. Perhaps a combination of qualitative VBCM models for identity S_N2 processes and Marcus theory for S_N2 cross reactions will prove useful as further investigations proceed.

Acknowledgment. We are grateful to the National Science Foundation and to the Stanford Data Center for support of this research. We thank Drs. R. G. Gilbert and S. C. Smith for giving us a copy of their RRKM program and for helpful discussion regarding the details of the theory. We also thank J. L. Wilbur for help with the experimental thermodynamic measurements and Dr. A. G. Császár for helpful discussion concerning the computational details.

Registry No. Cl^-, 16887-00-6; $ClCH_2CN$, 107-14-2; CH_3Cl, 74-87-3; Cl_2, 7782-50-5; $^{37}Cl^-$, 42150-36-7.

Supplementary Material Available: Tables of total electronic energies for all ab initio calculations along with the complete SQM force field for $ClCH_2CN$, the C_s- and C_1-symmetry chloride complexes, and the S_N2 transition state (10 pages). Ordering information is given on any current masthead page.

(154) Shi, Z.; Boyd, R. J. *J. Am. Chem. Soc.* **1989**, *111*, 1575.
(155) Miller, K. J.; Savchuik, J. A. *J. Am. Chem. Soc.* **1979**, *101*, 7206.
(156) McClellan, A. L. *Tables of Experimental Dipole Moments*; Rahava Enterprises: El Cerito, CA, 1974; Vol. 2, p 45.
(157) Wolfe, S.; Mitchell, D. J.; Schlegel, H. B. *J. Am. Chem. Soc.* **1981**, *103*, 7692.
(158) Johnston, H. S. *Gas Phase Reaction Rate Theory*; Ronald Press: New York, 1966.
(159) Dunitz, J. D. *Phil. Trans. R. Soc. London, Ser. B* **1975**, *272*, 99.
(160) Agmon, J. *Chem. Soc., Faraday Trans. 2* **1978**, *74*, 388.
(161) Pauling, L. *J. Am. Chem. Soc.* **1947**, *69*, 542.

Strong Interactions of Anionic Peptides and Alkaline Earth Metal Ions: Metal-Ion-Bound Peptides in the Gas Phase

Peifeng Hu and Michael L. Gross*

Contribution from the Midwest Center For Mass Spectrometry, Department of Chemistry, University of Nebraska—Lincoln, Lincoln, Nebraska 68588-0304. *Received March 18, 1992*

Abstract: Tripeptides comprising amino acids with neutral side chains interact with alkaline earth metal ions to form gas-phase anionic complexes of the composition [tripept + Met^{2+} − $3H^+$]$^-$ under fast atom bombardment. The metal ion binds to the deprotonated C-terminal carboxylate group and to the two amide nitrogens. Because the C-terminal and the central amino acid are tightly bound by the metal ion, they are not vulnerable to collisionally activated decompositions in a tandem mass spectrometer. Instead, the significant fragmentations occur at the N-terminal amino acid site, which is the least tightly bonded. Ions are formed by elimination of an imine and the imine plus CO from the N-terminus (product ions are assigned as x_2 + H and y_2, respectively). Other major fragmentations of this complex include dehydrogenation and loss of an ammonia molecule. Peptides with functionalized side chains, such as those of serine, threonine, and phenylalanine, lose the side chains readily when they are bound to metal ions and submitted to collisional activation. Other fragmentation channels are largely suppressed, indicating direct metal ion–side chain interaction. Fragmentation mechanisms are proposed on the basis of results with isotopically labeled peptides and from MS/MS/MS experiments.

Introduction

Tandem mass spectrometric (MS/MS) studies of peptides have gained momentum recently owing principally to the capacity for peptide sequencing. N-Blocked and other modified peptides can be readily sequenced by applying tandem mass spectrometry to desorbed $(M + H)^+$ ions.[1] Metal ion/peptide adducts have been

0002-7863/92/1514-9153$03.00/0